Desalination and Water Treatment
www.deswater.com
doi: 10.1080/19443994.2016.1144533

57 (2016) 25036–25056
November

Taylor & Francis
Taylor & Francis Group

Investigation of phosphate adsorption by a polyethersulfone-type affinity membrane using experimental and DFT methods

Xiuli Wang, Laizhou Song*, Feifei Yang, Jun He

College of Environmental and Chemical Engineering, Yanshan University, Qinhuangdao 066004, China, Tel. +86 3358387741; Fax: +86 3358061569; emails: xlwang790412@163.com (X. Wang), songlz@ysu.edu.cn (L. Song), Tel. +86 3358061422; Fax: +86 3358061569; email: 1576976391@qq.com (F. Yang), Tel. +86 3358387741; Fax: +86 3358061569; email: hejun@ysu.edu.cn (J. He)

Received 29 August 2015; Accepted 17 January 2016

ABSTRACT

A fabricated polyethersulfone (PES)-type affinity membrane was employed for the removal of phosphate from the aqueous solution. Influences of pH, contact time, temperature, and initial phosphate concentration, as well as the coexistent Cl^-, SO_4^{2-}, Ca(II), and Mg(II) on the phosphate adsorption were evaluated. The adsorption kinetics and the adsorption isotherms of this membrane toward phosphate were investigated. In addition, the insight into the phosphate uptake at an atomic-scale was revealed by the density functional theory calculations. The coexistent Cl^- and SO_4^{2-} showed a disturbance on the uptake of phosphate; conversely, the presence of Ca(II) and Mg(II) increased the uptake of phosphate. The negative influence of SO_4^{2-} was more remarkable than that of Cl^- due to the notably nucleophilic nature of this anion. The accelerating role of Ca(II) was stronger than that of Mg(II), because the Ca(II)-loaded membrane exhibited a more stronger affinity to phosphate than the Mg (II)-loaded form. Lagergren second-order and Langmuir models were suitable for describing the adsorption kinetics and adsorption isotherms, and the phosphate adsorption onto the membrane was a spontaneous and endothermic process.

Keywords: Phosphate; Adsorption; Polyethersulfone-type affinity membrane; Density functional theory; Coexistent ion

1. Introduction

The existent phosphate in aquatic environment is an essential nutrient for the growth of biological organisms. However, the excessive presence of this nutrient has been validated to result in the eutrophication, thereby causing the deterioration of water bodies [1,2]. The eutrophication caused by the excessive phosphate can lead to the intense accumulation of algae and the overgrowth of phytoplankton; thus, the incidents of oxygen lack and the decline of aquatic life will occur. It is well known that some neuro- and hepatotoxins produced by the eutrophication process can be released into water, and pose harm to aquatic animals, livestock, and human being [3,4]. The eutrophication will take place as the existent phosphate in water bodies is higher than 0.02 mg/l [5]. According to the published discharge standards of pollutants for municipal wastewater treatment plant (GB 18918-2002), the discharged concentration of total phosphorus in China should be no more than

*Corresponding author.

0.5 mg P/l. Therefore, techniques competent for the removal of phosphate should be developed before the effluents are discharged into natural water bodies.

To guarantee the concentration of phosphate consistent with the discharge standard, numerous techniques such as biological treatment [6], chemical precipitation [7], ion exchange [8,9], and adsorption process [10,11] have been employed to remove this pollutant from wastewater. Of all the techniques mentioned above, the adsorption process is an efficient and economical approach for the removal of phosphate. In particular, this technique is suitable for the recovery of phosphate from the dilute solution. Thus, enormous powder-like adsorbents involving fly ash [12], zeolite [13], calcite [14], ferrihydrite [15], bamboo charcoal [16], red soil [17], cellulose bearing the amine group [18], and the functional materials bearing metal-complexing groups [5,19,20] have been extensively applied for the removal of phosphate. Among the functional groups anchored to surfaces of the adsorbents, the amino group can be easily protonated [18], and thus shows a strong affinity to phosphate via the electrostatic attraction.

It has been widely accepted that the powder-like adsorbents show a high uptake of phosphate; whereas, it should be mentioned that they are not easily recovered for reuse. In contrast with adsorption processes of these adsorbents, the membrane separation technique with advantages of low pressure loss and easy scale-up [21,22] may be an appropriate method employed to remove phosphate from solutions. To our knowledge, insufficient efforts have been made focusing on the removal of phosphate by the membrane adsorption process. Of all the membrane techniques, although electrodialysis, polymer-enhanced ultrafiltration, nanofiltration, and reverse osmosis are competent for the removal of phosphate, applications of them have been limited because of the high costs and the strict pretreatments. In comparison with these membrane techniques, the conventional microfiltration and ultrafiltration processes show the excellence of high permeation flux, inexpensive investment, and needless strict pretreatments. These two kinds of membrane techniques might be the recommendable candidates applied for the removal of phosphate; unluckily, these two membrane techniques are not applicable to the removal of the dissolvable phosphate. Thus, the microfiltration- or ultrafiltration membrane bearing the amino group deserves to be explored for the removal of phosphate.

In addition, although adsorption experiments have provided considerable information about the kinetics and thermodynamics of adsorbents, atomistic details in the adsorbed structure of the adsorbent, and the immanent interaction between the solute and the absorbent are limited. The density functional theory (DFT) simulation, as a main supplement of the experimental method, has been extensively employed to reveal various chemical problems [23,24]. Some studies in phosphate adsorption via the DFT calculation have been reported [25–28]; whereas, few reports related to the DFT simulation focusing on the phosphate adsorption by the PES-type membrane can be found.

In this study, a polyethersulfone (PES)-type affinity membrane was synthesized via the chloroacetylation and amination processes. The fabricated affinity membrane was characterized by the techniques of scanning electron microscopy (SEM), energy dispersive X-ray spectrometry (EDS), Fourier transform infrared spectroscopy (FTIR), X-ray photoelectron spectrum (XPS), and nuclear magnetic resonance spectroscopy (NMR). Detailed studies regarding the effects of pH, contact time, temperature, and initial phosphate concentration on the phosphate adsorption by the membrane were carried out. Influences of Cl^-, SO_4^{2-}, Ca(II), and Mg(II) on the phosphate uptake were also studied. The batch adsorption experiments with respect to the kinetics and isotherms were performed in the presence of the above-mentioned four ions. The reused property of the membrane was also evaluated. Furthermore, the adsorption characteristics of the PES-type affinity membrane toward phosphate, and effects of the above four ions on the phosphate uptake were elucidated by the DFT simulations. Herein, DFT descriptors including chemical potential (μ), hardness (η), and global electrophilicity (ω) were calculated to investigate the chemical reactivity of the PES-type affinity membrane, phosphate, and the four ions mentioned above. The condensed Fukui function (FF) was calculated to explore the reactive sites of the affinity membrane and phosphate. In addition, the charge transfer (ΔN), the adsorption energies (ΔE_{ads}), and the Gibbs free energies of adsorption (ΔG_{ads}) between the aforementioned species were calculated.

2. Material and methods

2.1. Material

Polyethersulfone (PES, Ultrason E6020) powders with a molecular weight of ca. 58,000 were provided by BASF (Ludwigshafen, Germany). Analytical grade reagents involving absolute ethanol, anhydrous aluminum chloride, chloroform, chloroacetyl chloride, diethylenetriamine (DETA), N-N-dimethylacetamide (DMAc), polyvinylpyrrolidone (PVP), hydrochloric acid (37 wt.%), $NaH_2PO_4{\cdot}2H_2O$, NaCl, NaOH,

$CaCl_2{\cdot}2H_2O$, $MgCl_2{\cdot}6H_2O$, and $Na_2SO_4{\cdot}10H_2O$ (purchased from Jingchun Scientific Co., Ltd. Shanghai, China) were used as received. The stock solution of phosphate (1 g P/l) was prepared and the working solutions containing 20–120 mg P/l were prepared by diluting the stock solution to appropriate volumes. All concentrations of stock solutions containing Cl^-, SO_4^{2-}, Ca(II), and Mg(II) were 1.0 mol/l.

2.2. Preparation of the PES-type affinity membrane

The preparation process of PES-type affinity membrane (described as DETA-PES) was illustrated in Fig. 1. First of all, 6 g of PES powders were dissolved in 90 ml of chloroform, and then 5 g of anhydrous aluminum trichloride was slowly added into this solution. After the mixed solution was magnetically stirred for 30 min at room temperature, 4 ml of chloroacetyl chloride was dropped into the mixed solution. The temperature of this solution was kept at 313 K under the protection atmosphere of nitrogen gas with a flow rate of 30 ml/min. Four hours later, 150 ml of absolute ethanol was added to the above solution to obtain the sediment-type chloroacetylated PES powders. Then, the chloroacetylated PES powders were washed using absolute ethanol to remove chloroform, and the excessive anhydrous aluminum trichloride and chloroacetyl chloride. In the end, the cleaned powders were dried at 333 K for 6 h.

The as-prepared chloroacetylated PES powders were dissolved in 30 ml of DMAc at a temperature of 353 K. After that, 3 ml of DETA was added into the solution, and the temperature of this solution was increased to 403 K. After 4 h, the temperature of the solution was reduced to 353 K and 0.7 g of PVP was added. This mixed solution was magnetically stirred at this temperature for another 4 h. Lastly, the PES-type affinity membrane (DETA-PES) was prepared via a phase inversion process, and this membrane was cleaned with deionized water and kept for a series of characterizations and adsorption tests.

2.3. Membrane characterization

The morphologies of the DETA-PES affinity membrane were characterized using a SEM (XL30, Philips, Amsterdam, Netherlands) incorporated with an EDS (ISIS300, Philips) for determining elements of the membrane. The FTIR spectra of the membrane before and after phosphate adsorption were determined by an E55 + FRA106 FTIR spectrometer (Bruker, Karlsruhe, Germany). An X-ray photoelectron spectroscopy (XPS) (VG ESCA250, Thermo Fisher, Waltham, MA) was used to characterize the elements existing on the membrane after the static bath adsorption of phosphate. The solid-state NMR spectra of the membrane before and after phosphate uptake were characterized with a nuclear magnetic resonance spectrometer (Bruker Avance III 400, Karlsruhe, Germany). In addition, the mean pore size of the affinity membrane was measured by the water permeability method [29]. The point of zero charge (pH_{pzc}) of the membrane was determined by a batch equilibration method [30].

2.4. Adsorption experiments

The batch adsorption experiments were performed in 100 ml of phosphate solutions; the addition of DETA-PES affinity membrane was ~0.1 g. The effect of pH ranging from 2.0 to 12.0 on the phosphate uptake of the affinity membrane was examined, and the determined optimum pH from this test was adopted for all experiments. During the test, the pHs of the solutions were adjusted using hydrochloric acid and sodium hydroxide solutions with the concentrations of 1.0 mol/l. In addition, effects of the contact time (0–340 min), the temperature (288, 298, and 308 K), and

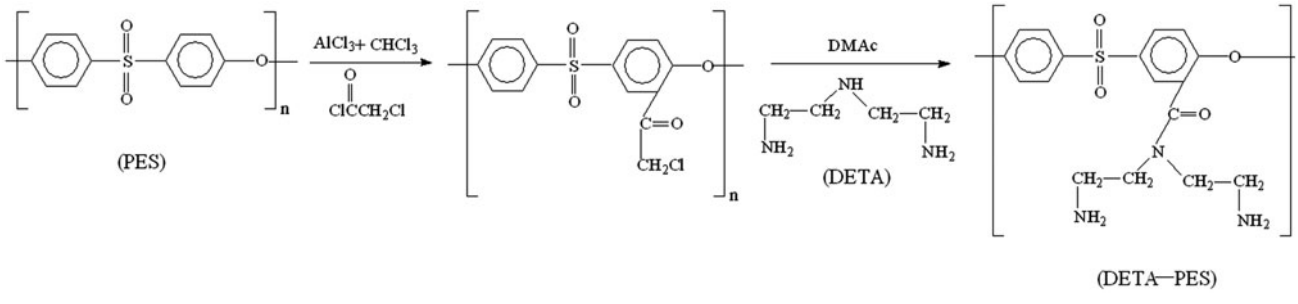

Fig. 1. Preparation process of the DETA-PES affinity membrane.

the initial phosphate concentration (20–120 mg P/l) were studied.

In order to elucidate the effects of Cl^-, SO_4^{2-}, Ca(II), and Mg(II), the phosphate uptakes of the membrane were measured with the coexistence of these four ions at different concentrations (0–0.1 mol/l). The adsorption tests were conducted at 298 K in the solutions containing 80 mg P/l of phosphate. For each test at different time intervals (i.e. 10, 30, and 60 min), 1 ml of liquor was withdrawn from the solution to determine the residual phosphate till equilibrium. The concentration of phosphate was determined by the colorimetrical method, using a visible light spectrophotometer (722s, Tianxiang Co., Ltd, shanghai, China). This measurement is based on a blue complex formed by the interaction between molybdate solution and ascorbic acid mixture, and the measurement wavelength was 700 nm. The amounts of phosphate adsorption by the affinity membrane were calculated via Eq. (1) [31,32]:

$$q_t = \frac{(c_0 - c_t) \times V}{M} \quad (1)$$

where q_t is the uptake of phosphate of a unit weight of the membrane (mg P/g) at time t; c_0 is the initial concentration of phosphate (mg P/l), and c_t is the phosphate concentration at time t in the aqueous solution (mg P/l). V and M are the volume of the aqueous phase (l) and the dry weight of the affinity membrane (g), respectively.

As to the single-phosphate system, adsorption kinetics was investigated at 298 K; the initial phosphate concentration, and the value of pH were kept at 80 mg P/l, and 4.0. The adsorption kinetics of Cl^-, SO_4^{2-}, Ca(II), and Mg(II) coexisting systems were also studied. The phosphate concentration was 80 mg P/l and the concentrations of these four coexistent ions were 0.04 mol/l. For the single-phosphate and the four ions coexisting systems, adsorption equilibrium tests were examined at 298 K in one experiment at different initial phosphate concentrations (20–120 mg P/l). The concentrations of phosphate at initial stage and equilibrium were then measured. The amounts of Cl^-, SO_4^{2-}, Ca(II), and Mg(II) were equivalent to those of the kinetics tests.

2.5. Adsorption/desorption experiment

The reused property of DETA-PES affinity membrane was measured using the 0.1 mol/l of NaOH solution as the elution agent. The membrane with a dry weight of ~0.1 g loading the phosphate was immersed in the NaOH solution. The adsorption/desorption processes for the same membrane were repeated five times. The amounts of phosphate adsorbed and eluted during the adsorption/desorption processes were determined. The desorption efficiency (DE) was evaluated using Eq. (2) [33]:

$$DE = (q_1/q_0) \times 100\% \quad (2)$$

where q_1 is the desorbed amount of phosphate from the membrane (mg P/g) in the desorption process, q_0 is the adsorbed amount of phosphate on the membrane at equilibrium (mg P/g).

2.6. Computational details

All calculations based on DFT were implemented in the Materials Studio DMol^3 (version 7.0, Accelrys Inc., San Diego, USA) [34]. The structural optimization was performed at the generalized gradient approximation (GGA) level with the spin unrestricted approach. Double numerical plus polarization functions (DNP) and Becke exchange functional in conjunction with the Lee–Yang–Parr correlation functional (BLYP) were employed. Pulay's direct inversion in the iterative subspace (DIIS) technique and the small electron thermal smearing with a value of 0.005 Ha were employed to accelerate self-consistent field (SCF) convergence. Frequency calculations and Mulliken population analyses were performed to obtain the geometrical and energetic parameters. A continuum salvation model (COSMO) was used due to the aqueous adsorption, and the dielectric constant of water was set as 78.54. In addition, the TS (Tkatchenko-Scheffler) method for DFT-D correction was employed in terms of the weak interactions such as hydrogen bond and van der Waals force.

The optimized structures for the unit of the PES-type membrane grafted by the DETA group (DETA-PES), phosphate, Cl^-, SO_4^{2-}, Ca(II), and Mg(II) are shown in Fig. 2. The geometries of phosphate, Cl^-, and SO_4^{2-} in the form of $H_2PO_4^-$, $[Cl(H_2O)_5]^-$, and HSO_4^- were adopted, respectively. The calculated configuration of Ca(II) was similar to that of Mg(II); both of them are in the form of $[M(II)(H_2O)_6]^{2+}$ (M(II) represents Ca(II) or Mg(II)).

3. Results and discussion

3.1. Characterization of the PES-type affinity membrane

3.1.1. SEM and EDS analyses

The surface and sectional morphologies of DETA-PES affinity membrane are presented in Fig. 3. As

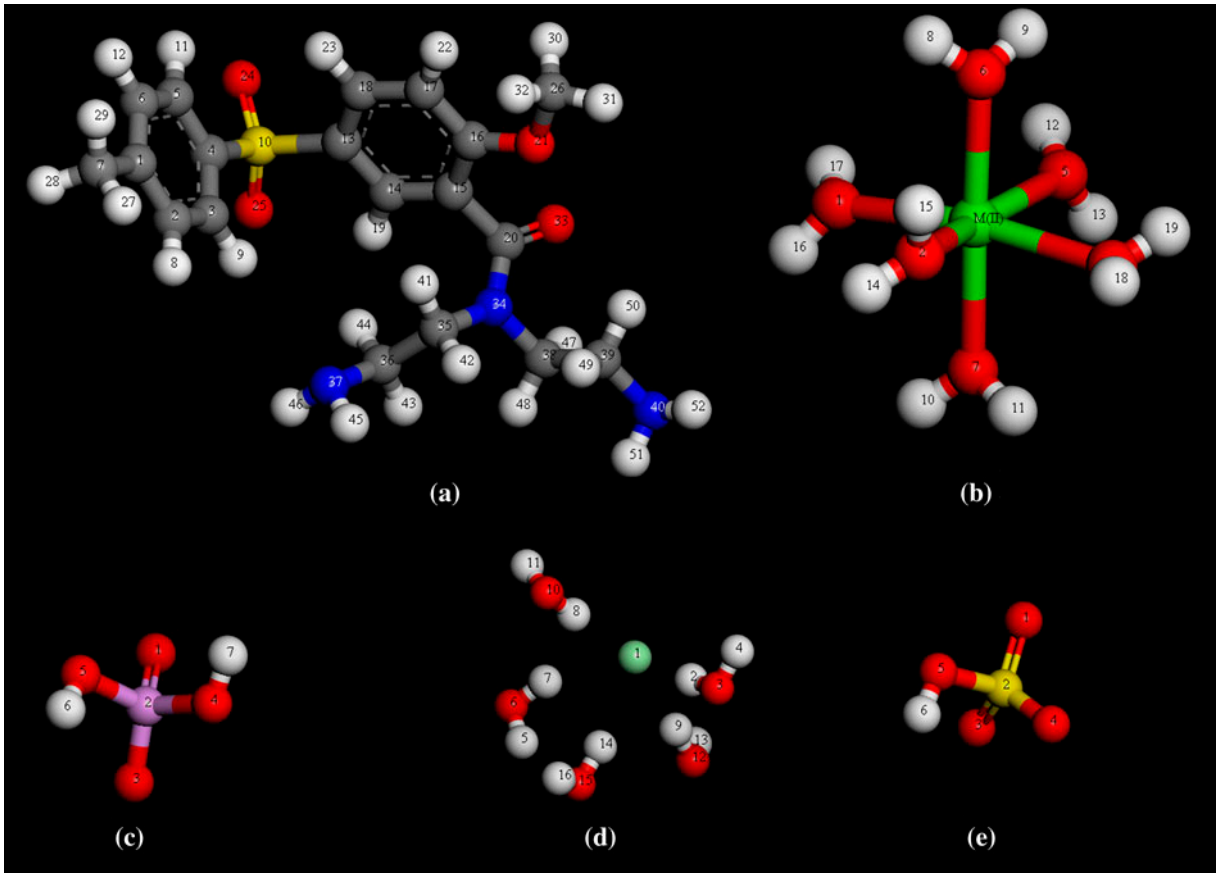

Fig. 2. Optimized structures for the unit of the affinity membrane, Ca(II) and Mg(II), phosphate, Cl^-, and SO_4^{2-} with the atoms numbering scheme adopted in this study: atom types are denoted by sequence number as follows: (a) the unit of the affinity membrane (8, 9, 11, 12, 19, 22, 23, 27–32, 41–52—hydrogen; 1–7, 13–18, 20, 26, 35, 36, 38, 39—carbon; 21, 24, 25, 33—oxygen; 34, 37, 40—nitrogen; 10—sulfur), (b) Ca(II) and Mg(II) (M(II) represents Ca(II) or Mg(II); 8–19—hydrogen; 1, 2, 4–7—oxygen), (c) phosphate (6, 7—hydrogen; 1, 3–5—oxygen; 2—phosphorus), (d) Cl^- (2, 4, 5, 7–9, 11, 13, 14, 16—hydrogen; 3, 6, 10, 12, 15—oxygen; 1–chlorine), and (e) SO_4^{2-} (6—hydrogen; 1, 3–5—oxygen; 2—sulfur).

shown in Fig. 3(a), the membrane possesses a uniform microporous structure. The determined average size of the micropore is 0.18 μm, which will be helpful for the permeation of solutions through this membrane. As indicated by the sectional morphology (Fig. 3(b)), the finger-like pores (labeled by circles) can be observed near the surface layer of the membrane; the floc-shaped porous structures (described by a rectangle) are also found in the inner of the membrane. Before and after phosphate adsorption, the EDS spectra of DETA-PES affinity membrane were examined, and the results are displayed in Fig. 3(c) and (d). Compared with EDS before phosphate adsorption (Fig. 3(c)), in addition to carbon, nitrogen, oxygen, and sulfur elements, phosphorus element is also detected after the phosphate adsorption (Fig. 3(d)), suggesting the phosphate uptake of the membrane.

3.1.2. FTIR analysis

The FTIR spectra of PES powder, DETA-PES affinity membrane before and after phosphate adsorption are shown in Fig. 4. For the spectrum of DETA-PES membrane (Fig. 4(b)), except for the peaks at 1,143, 1,296, and 1,321 cm^{-1} corresponding to the S=O group [35,36], two peaks at 1,656 and 3,436 cm^{-1} can be attributed to the $–NH_2$ group stretching vibration [18,37,38], thus indicating that the DETA group is successfully grafted onto the PES polymer. The peak at 1,049 cm^{-1} can be assigned to the phosphate group [18], suggesting the phosphate uptake of the affinity membrane. After the phosphate adsorption, the peak appearing at 1,656 cm^{-1} shifts to 1,660 cm^{-1}, which may be due to the electrostatic attraction interaction between the primary amine group of the membrane and phosphate [18].

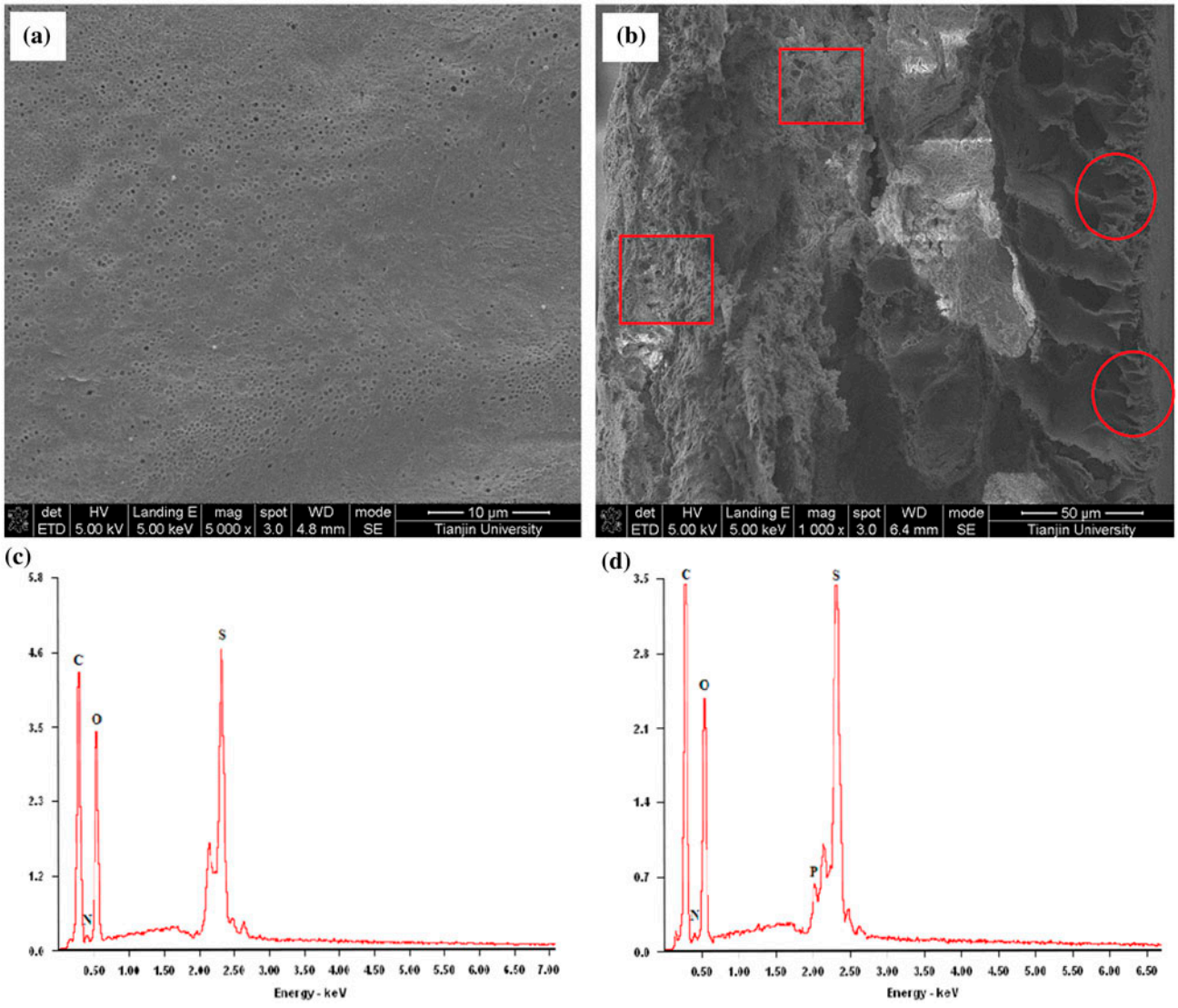

Fig. 3. SEM morphologies and EDS spectra of DETA-PES affinity membrane: (a) surface morphology, (b) section morphology, (c) EDS spectrum before phosphate adsorption, and (d) EDS spectrum after phosphate adsorption.

3.1.3. XPS analysis

In order to further investigate the surface chemical compositions of the DETA-PES affinity membrane, XPS measurements were performed. The full XPS spectra of the affinity membrane before and after phosphate adsorption are depicted in Fig. 5. The photoelectron lines at binding energy of 27.2, 171.2, 235.2, 288.0, 402.4, and 535.2 eV are described to O 2s, S 2p, S 2s, C 1s, N 1s, and O 1s, respectively [39–41]. The detected nitrogen element implies the presence of DETA group. Also, as shown in Fig. 5(b), the peak appearing at 134.0 eV (the inset figure) can be attributed to existence of phosphate [42]. On the basis of this fact, it can be inferred that phosphate was adsorbed by the protonated amino group existing on the surface of DETA-PES membrane.

In addition, the high-resolution spectra of N 1s before and after phosphate adsorption were analyzed (Fig. 5(c) and (d)). Before phosphate adsorption, the peaks at 399.2 and 400.4 eV (Fig. 5(c)) correspond to $–NH_2$ and C–N groups [43], respectively. After phosphate adsorption (Fig. 5(d)), these two peaks shift from 399.2 to 399.6 eV, and from 400.4 to 401.2 eV. This can be due to the electrostatic attraction interaction between the protonated amino group and phosphate [44].

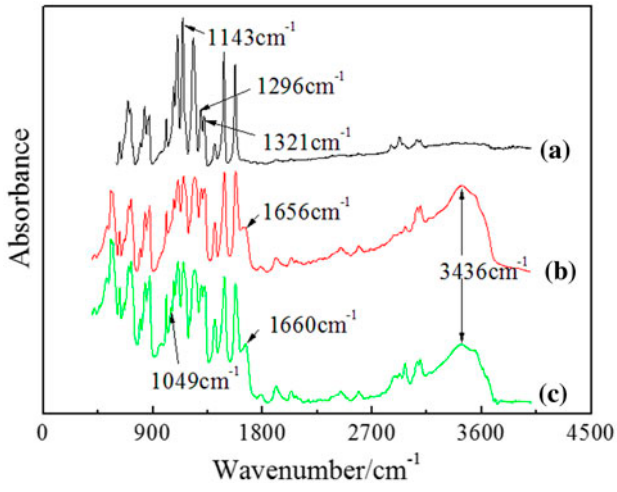

Fig. 4. FTIR spectra: (a) PES powder, (b) DETA-PES affinity membrane before phosphate adsorption, and (c) DETA-PES affinity membrane after phosphate adsorption.

3.1.4. NMR analysis

The ^{13}C and ^{31}P solid-state NMR spectra of DETA-PES affinity membrane before and after phosphate adsorption are depicted in Fig. 6. As to the ^{13}C NMR spectrum (Fig. 6(a)), the peaks at 121.7, 129.8, 136.8, and 159.3 ppm are attributed to the benzene ring carbon atoms of PES polymer [45,46]. The peak appearing at 176.3 ppm is attributed to the acylamide group [32,33]; the peaks at 43.1 and 69.5 ppm can be assigned to the carbon of $–CH_2N–$ group [32,33], indicating that the DETA group is grafted into the PES polymer. After the phosphate adsorption, the intensity of the peak appearing at 176.3 ppm decreases, which may be due to the interaction between the protonated amino group and phosphate. In addition, compared with the ^{31}P NMR spectrum before the phosphate adsorption, an obvious peak appearing at −5.83 ppm (Fig. 6(b)) after the uptake of phosphate can be detected; this peak can be owned to the existence of

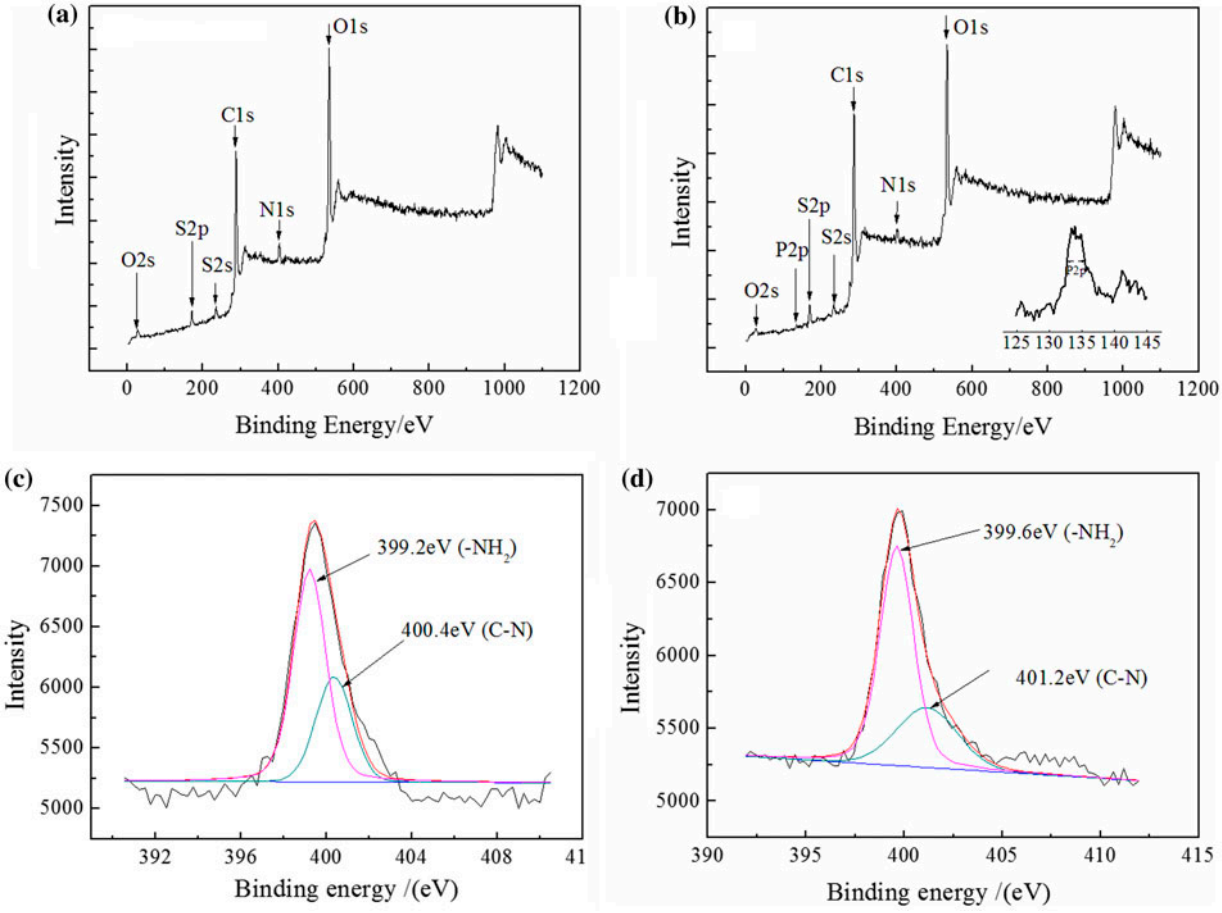

Fig. 5. XPS spectra of DETA-PES affinity membrane: (a) before phosphate adsorption, (b) after phosphate adsorption, (c) N 1s spectrum before phosphate adsorption, and (d) N 1s spectrum after phosphate adsorption.

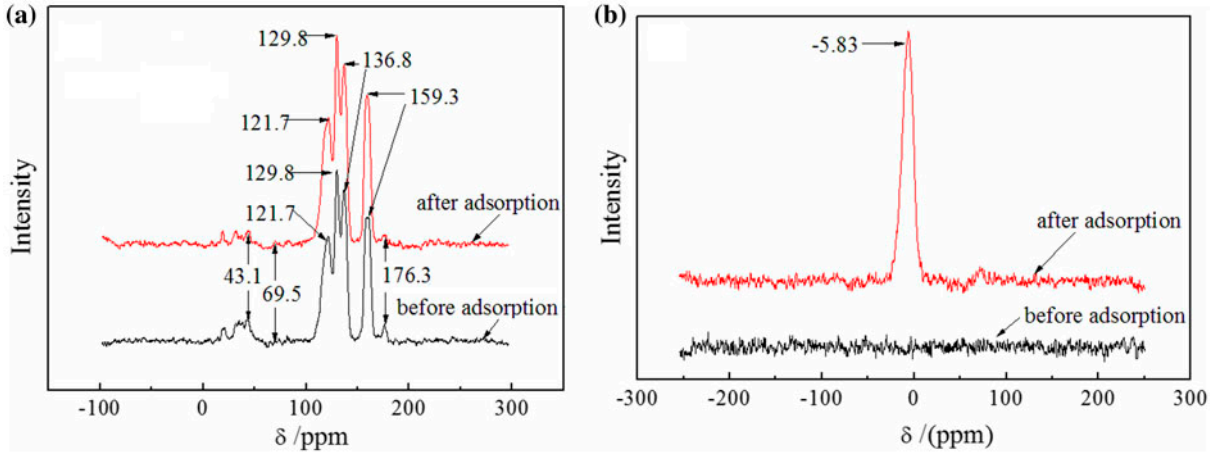

Fig. 6. Solid-state NMR spectra: (a) ^{13}C NMR of DETA-PES affinity membrane and (b) ^{31}P NMR of DETA-PES affinity membrane.

phosphate [47,48]. Thus, it can be confirmed that phosphate is adsorbed by the DETA-PES affinity membrane, thereby achieving the removal of phosphate from aqueous solutions.

3.2. Effects of basic variables

The pH of the aqueous solution will play an important role in the adsorption process, so the effect of pH on the phosphate uptake of the affinity membrane was investigated. The phosphate uptake of the DETA-PES affinity membrane is strongly dependent on the value of pH (Fig. 7(a)). The phosphate uptake of the DETA-PES membrane increases when pH rises from 2.0 to 4.0. The optimal pH for the phosphate adsorption is 4.0. Thus, phosphate is removed by the membrane in the form of $H_2PO_4^-$ [38,49]. The determined point of zero charge (pH_{pzc}) is 4.2, so the surface of the membrane will be negative as pH value is higher than this value; on the contrary, it will become positive. As pH is in the range of 2.0–4.0, the nitrogen atoms of the amino group are protonated, and this will be of benefit for the uptake of phosphate. However, when pH is lower than 4.0, a part of $H_2PO_4^-$ anions will become H_3PO_4 molecules; also, phosphate will be existent in the form of H_3PO_4 as pH is smaller than 2.0. These facts can result in the decrease in the phosphate uptake of the membrane. In addition, as pH is larger than 4.0, the deprotonated amino group of the membrane can reduce the affinity to phosphate, thereby resulting in the decrease of phosphate adsorption. Herein, in comparison with the DETA-PES affinity membrane, it should be mentioned that the original PES membrane with a pH_{pzc} value of 5.6 shows little uptake of phosphate, and this can be due to the nonexistence of the amino group.

The phosphate uptake of DETA-PES affinity membrane as a function of time at different temperatures is shown in Fig. 7(b). It can be seen the equilibrium time for phosphate adsorption by the affinity membrane is 280 min. In this adsorption process, two stages including rapid and slow stage can be observed. The rapid adsorption occurs within the first 90 min, and the slow uptake of phosphate extends the remaining 190 min. At the beginning of the uptake of phosphate, there are plentiful spare sites on the membrane, and this will be beneficial to the phosphate adsorption [50]. In the remaining 190 min, the loss of adsorption sites will reduce the uptake of phosphate. In addition, as demonstrated by Fig. 7(b), the temperature exhibits a positive influence on the phosphate adsorption, and the uptake of phosphate increases from 41.9 to 50.8 mg P/g as the temperature rises from 288 to 308 K. Thus, the phosphate uptake of DETA-PES membrane is an endothermic process.

The phosphate uptake of DETA-PES membrane increases significantly with increasing concentration of the initial phosphate (Fig. 7(c)). The phosphate uptake of the membrane at 298 K rises from 15.1 to 52.2 mg P/g, when the initial phosphate concentration increases from 20 to 120 mg P/l. However, the removal efficiency of phosphate reduces from 75.6 to 43.5%. Herein, the initial phosphate concentration of 80 mg P/l was ascertained for all the following experiments.

3.3. Effects of the coexistent ions

Cl^-, SO_4^{2-}, Ca(II), and Mg(II) are the common ions in the solution, and they will interfere in the adsorption of phosphate. Hence, the effects of these four ions with different concentrations on phosphate adsorption of the affinity membrane were investigated. The effects

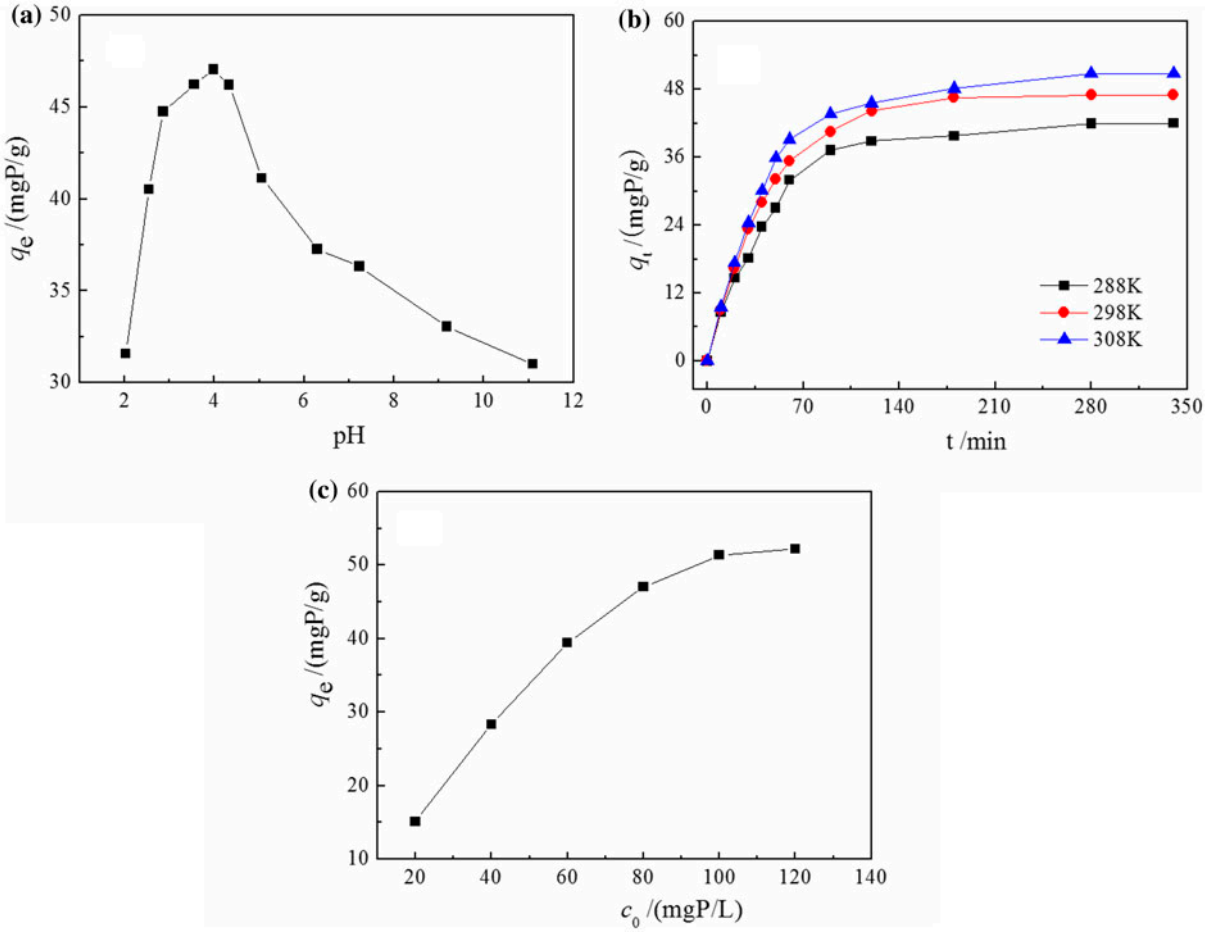

Fig. 7. Effects of pH, temperature, contact time, and initial phosphate concentration on phosphate adsorption by the DETA-PES affinity membrane: (a) pH (c_0(phosphate) =80 mg P/l; t: 360 min; membrane dry weight: 0.1 g; T: 298 K); (b) temperature and contact time (c_0(phosphate) = 80 mg P/l; membrane dry weight: 0.1 g; pH 4.0); (c) initial phosphate concentration (membrane dry weight: 0.1 g; pH 4.0; t: 360 min; T: 298 K).

of coexistent Cl^- and SO_4^{2-} on the phosphate uptake are displayed in Fig. 8(a). As indicated by Fig. 8(a), the phosphate uptake of DETA-PES membrane decreases with the increasing concentrations of these two anions. Thus, the coexistence of Cl^- and SO_4^{2-} shows a negative effect on the adsorption of phosphate. The coexistent Cl^- and SO_4^{2-} with a concentration of 0.1 mol/l reduce the phosphate uptakes of the membrane by 8.8 and 11.2%, respectively. Thus, the disturbance of Cl^- is inferior to that of SO_4^{2-}. The negative effects of Cl^- and SO_4^{2-} on the uptake of phosphate can be attributed to the competitive adsorption between these two anions and phosphate. In spite of the coexistence of these two anions, it should be mentioned that the phosphate uptake of the DETA-PES affinity membrane still dominates the adsorption process.

As the concentrations of Ca(II) and Mg(II) rise from 0 to 0.04 mol/l, the uptakes of phosphate increase significantly (Fig. 8(b)). The increasing trend of the phosphate uptake becomes slight when the concentrations of them increase from 0.04 to 0.1 mol/l. This can be explained as follows: Ca(II) and Mg(II) can be coordinated by the amino groups of the affinity membrane, and the affinities between the membrane and these two metals will increase as the concentrations rise from 0 to 0.04 mol/l. Then, the enhancements in their uptakes become slight with the increase in concentrations of them. These two adsorbed metals onto the affinity membrane will be helpful in the uptake of phosphate [19]. The phosphate uptakes of DETA-PES membrane increase from 47.1 mg P/g to 55.4 and 51.2 mg P/g as Ca(II) and Mg(II) coexist with a concentration of 0.04 mol/l. Therefore, the positive effect of these two metal cations on the uptake of phosphate is in the order of Ca(II) > Mg(II).

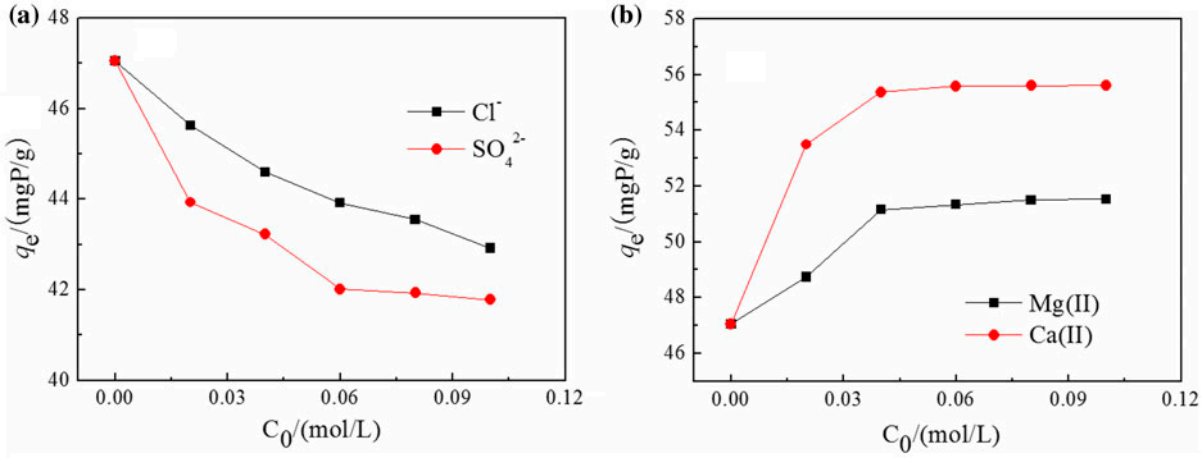

Fig. 8. Effect of the existent ion concentration on phosphate adsorption: (a) Cl^- and SO_4^{2-}; (b) Ca(II) and Mg(II): c_0(phosphate) = 80 mg P/l; t: 360 min; membrane dry weight: 0.1 g; T: 298 K; pH 4.0.

3.4. Studies of adsorption kinetics and adsorption isotherm

The adsorption kinetics and adsorption isotherm play an important role in evaluating of the sorption process. Herein, the adsorption kinetics and adsorption isotherm of the affinity membrane toward phosphate in the single-phosphate, phosphate–Cl^-, phosphate–SO_4^{2-}, phosphate–Ca(II), and phosphate–Mg(II) systems were studied.

The phosphate uptakes as a function of time for single-phosphate, phosphate–Cl^-, phosphate–SO_4^{2-}, phosphate–Ca(II), and phosphate–Mg(II) systems are illustrated in Fig. 9(a). Compared with the single-phosphate system, the coexistent Cl^- and SO_4^{2-} decrease the phosphate uptakes of the membrane; conversely, the phosphate uptakes of phosphate–Ca(II) and phosphate–Mg(II) two systems are enhanced. The experimental kinetics data for the above five systems are analyzed by Lagergren first-order and Lagergren second-order equations [33,51]. The obtained parameters are listed in Table 1. Where q_{et} (mg P/g) is the amount of adsorbed phosphate at equilibrium; k_1 (1/min) and k_2 (g/(mg P min)) are the rate constants of these two kinetic equations. As indicated by Table 1, in view of the coefficient of determination, the Lagergren second-order adsorption model is more suitable than the Lagergren first-order model for describing the adsorption kinetics of the membrane toward phosphate. Thus, the chemisorption may play a more important role than physisorption in the phosphate uptake of DETA-PES membrane [52]. By the comparison of k_2 and q_{et}, it can be concluded that the disturbance of the two coexistent anions follows the order: $SO_4^{2-} > Cl^-$. The competitive adsorption between phosphate and the two coexistent anions accelerates the adsorption process, due to the large values of k_2 for phosphate–Cl^- and phosphate–SO_4^{2-} systems. In addition, with the coexistence of Ca(II) and Mg(II), k_2 of the single-phosphate and two cations coexisting systems follows the descending sequence of phosphate > phosphate–Mg(II) > phosphate–Ca(II), indicating the enhancements of Ca(II) and Mg(II) on the phosphate uptake of the membrane. Of course, the synergistic effect of Ca(II) on the phosphate adsorption is stronger than that of Mg(II).

The isotherm experimental data of single-phosphate, phosphate–Cl^-, phosphate–SO_4^{2-}, phosphate–Ca(II), and phosphate–Mg(II) five systems obtained at 298 K are shown in Fig. 9(b). The thermodynamic behaviors of the DETA-PES membrane toward phosphate are interpreted by Freundlich, Langmuir, and Dubinin–Radushkevich (D–R) isotherm models [51,53]. The analyzed parameters of these three models are tabulated in Table 2, where q_e (mg P/g) is the amount of phosphate adsorbed at equilibrium, q_m (mg P/g) is the maximum adsorption capacity of the affinity membrane. K_F and $1/n$ are the Freundlich constants related to the adsorption capacity and the adsorption intensity; b (l/mg P) is the Langmuir adsorption constant. E (kJ/mol) is the mean free energy of adsorption. Compared with Freundlich and D–R models, the Langmuir isotherm model is more competent than these two models for the description in the thermodynamic behavior of the membrane toward phosphate, because of its higher determination coefficients ($R^2 > 0.99$). Therefore, phosphate may be adsorbed in the form of monolayer onto the surface of the affinity membrane [37]. As shown by the data (Table 2), the value of q_m at 298 K derived from the Langmuir model is slightly

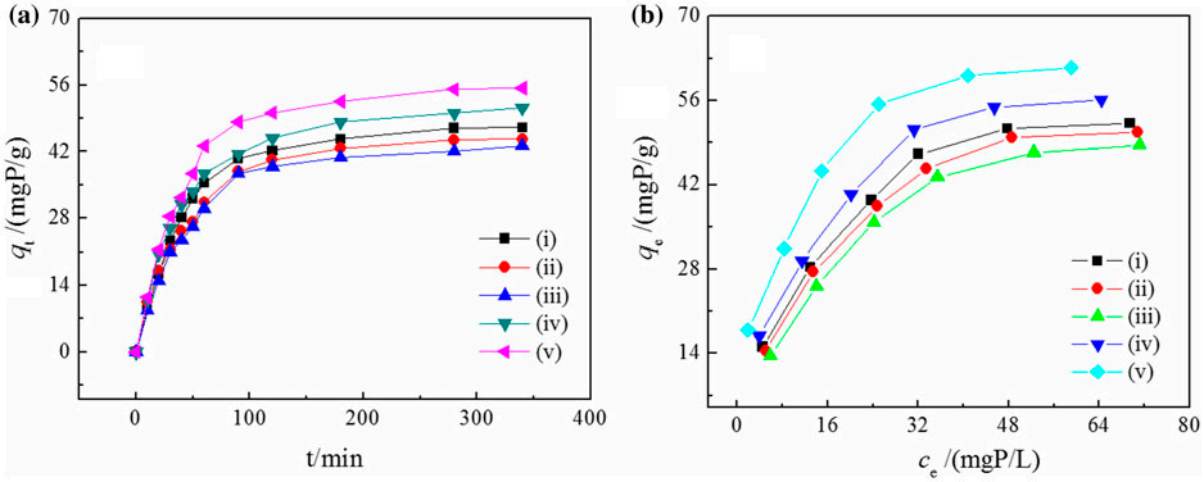

Fig. 9. Adsorption kinetics and adsorption isotherm for phosphate onto the DETA-PES membrane: (a) Adsorption kinetics: (i) single-phosphate, (ii) phosphate–Cl^-, (iii) phosphate–SO_4^{2-}, (iv) phosphate–Mg(II), (v) phosphate–Ca(II); (c_0(phosphate) = 80 mg P/l; $c_0(Cl^-) = c_0(SO_4^{2-}) = c_0$(Mg(II)) = c_0(Ca(II)) = 0.04 mol/l; T: 298 K; membrane dry weight: 0.1 g; pH 4.0); (b) Adsorption isotherm: (i) single-phosphate, (ii) phosphate–Cl^-, (iii) phosphate–SO_4^{2-}, (iv) phosphate–Mg(II), (v) phosphate–Ca(II); ($c_0(Cl^-) = c_0(SO_4^{2-}) = c_0$(Mg(II)) = c_0(Ca(II)) = 0.04 mol/l; t: 360 min; T: 298 K; membrane dry weight: 0.1 g; pH 4.0).

Table 1
Adsorption parameters for Lagergren first-order and Lagergren second-order models at 298 K

	Lagergren first-order model $\ln(q_e - q_t) = \ln q_{et} - k_1 t$			Lagergren second-order model $\frac{t}{q_t} = \frac{1}{k_2 q_{et}^2} + \frac{t}{q_{et}}$		
System	k_1 (/min)	q_{et} (mgP/g)	R^2	k_2 ($\times 10^{-4}$ g/(mgP min))	q_{et} (mgP/g)	R^2
Single-phosphate	0.021	46.59	0.985	5.18	53.02	0.998
Phosphate–Cl^-	0.024	52.63	0.981	5.51	49.90	0.999
Phosphate–SO_4^{2-}	0.015	32.87	0.980	5.52	47.87	0.998
Phosphate–Ca(II)	0.020	52.88	0.985	4.72	62.15	0.999
Phosphate–Mg(II)	0.014	38.33	0.990	5.08	56.72	0.999

Table 2
Adsorption parameters for Langmuir, Freundlich, and D–R models at 298 K

	Freundlich model $\log q_e = \log k_F + \frac{1}{n}\log c_e$			Langmuir model $\frac{c_e}{q_e} = \frac{1}{q_m b} + \frac{c_e}{q_m}$			D–R model $\ln q_e = \ln q_m - \frac{1}{2E^2}[RT\ln(1 + \frac{1}{c_e})]^2$		
System	K_F	$1/n$	R^2	q_m (mgP/g)	b (1/mg P)	R^2	q_m (mgP/g)	E (kJ/mol)	R^2
Single-phosphate	8.00	0.48	0.977	64.98	0.067	0.996	44.91	11.18	0.927
Phosphate–Cl^-	7.17	0.49	0.977	64.27	0.060	0.997	43.71	9.97	0.936
Phosphate–SO_4^{2-}	6.01	0.52	0.977	64.18	0.049	0.997	41.92	8.48	0.937
Phosphate–Ca(II)	14.45	0.38	0.984	70.08	0.130	0.997	50.24	26.81	0.878
Phosphate–Mg(II)	9.68	0.45	0.984	68.92	0.076	0.997	47.31	13.39	0.903

greater than the experimental value, which can be attributed to the fact that some adsorption sites of the membrane are unoccupied. q_m follows the order of phosphate–Ca(II) > phosphate–Mg(II) > phosphate > phosphate–Cl^- > phosphate–SO_4^{2-}, indicating the disturbances of Cl^- and SO_4^{2-} and the enhancing effects of Ca(II) and Mg(II). The increasing trend of b and q_m for phosphate–Ca(II) and phosphate–Mg(II) systems suggests the positive effects of these two cations following the trend: Ca(II) > Mg(II). Also, the

disturbances of the two anions following the order of $Cl^- < SO_4^{2-}$ can be validated. The value of $1/n$ is smaller than 1, which indicates that phosphate is easily adsorbed by the affinity membrane. In addition, all values of the mean free energy of adsorption (E) obtained from D–R isotherm model for the above-mentioned five systems are higher than 8.0 kJ/mol, thereby indicating the chemisorption characteristic of phosphate adsorption by the affinity membrane [32,54].

The phosphate uptakes of some reported adsorbents are summarized in Table 3. By a comparison of the phosphate uptake, the DETA-PES affinity membrane exhibits an excellent performance in the uptake of phosphate. Thus, we confirm that the fabricated DETA-PES affinity membrane will be competent for the removal of phosphate from aqueous solutions.

The thermodynamic parameters including standard free energy change (ΔG°), standard enthalpy change (ΔH°), and standard entropy change (ΔS°) were determined via the Eq. (3) [51], to elucidate the nature of phosphate adsorption by the affinity membrane:

$$\ln K_D = -\frac{\Delta H^\circ}{RT} + \frac{\Delta S^\circ}{R}, \quad \Delta G^\circ = \Delta H^\circ - T\Delta S^\circ \tag{3}$$

where K_D (ml/g) and R (8.314 J/(mol K)) are the distribution coefficient and the gas constant; T (K) is the absolute temperature. The calculated results of these three parameters are tabulated in Table 4. The negative ΔG° and the positive ΔH° display that the phosphate adsorption is a spontaneous and endothermic process. The positive ΔS° shows a slight increase in randomness during the adsorption process, this may be due to the release of water molecules from the hydrated phosphate.

3.5. Reused property of the affinity membrane

The reused property of DETA-PES affinity membrane is important for the potential engineering application. As indicated by Fig. 7(a), phosphate adsorption by the affinity membrane is small as the pH value is higher than 11. Therefore, the 0.1 mol/l of NaOH solution was adopted to regenerate the membrane. The adsorption/desorption cycles were conducted five times using the same membrane, and the results are represented in Fig. 10. After five cycles of adsorption/desorption processes, the adsorption capacity of the membrane shows a slight decrease (from 47.1 to 45.2 mg P/g); therefore, it can be recognized that the adsorption capacity of the membrane is well maintained. In addition, the DE of the membrane is higher than 96%. Based on this fact, the DETA-PES affinity membrane will be qualified for the practical application in the phosphate uptake from aqueous solutions.

3.6. DFT simulations

3.6.1. Protonation of the affinity membrane

Nitrogen atoms of the amino group anchored onto the surface of the DETA-PES affinity membrane will be protonated, as pH is kept at 4.0. This membrane

Table 3
Comparison in phosphate uptakes of different adsorbents

	Test condition					
Adsorbent	pH	Phosphate concentration (mg P/l)	Temperature (K)	Time (h)	Phosphate uptake (mg P/g)	Refs.
DETA-PES	4.0	20	298	6	15.1	This test
DETA-PES	4.0	80	298	6	47.1	This test
CeFP	5.0	62	303	9	43.9	[5]
S15-NN-Fe-0.5	3.0−6.0	80	308	4	20.7	[10]
Al-Bent	3.0	20	−	6	5.1	[11]
Cell-g-E/PEI	4.5	82	303	3	76.0	[18]
CS-Cu	5.0	100	298	7	28.9	[37]
La-NN-M41	7.0	33	298	4	14.6	[38]
ACF-La	4.0	25	293	6	8.54	[50]
$Nb_2O_5{\cdot}4H_2O$	2.0	16	298	5	2.8	[51]
SSW-Fe	7.0	30	303	24	22.1	[55]
DSTC	7.0	20	295	24	7.6	[56]
Fe-Mn binary oxide	5.6	10	298	24	8.3	[57]

Table 4
Adsorption thermodynamic parameters of the membrane toward phosphate at 298 K

System	ΔH° (kJ/mol)	ΔS° (kJ/(mol K))	ΔG° (kJ/mol)			R^2
			288 K	298 K	308 K	
Single-phosphate	15.09	0.053	−0.296	−0.704	−1.234	0.959
Phosphate–Cl^-	10.61	0.038	−0.260	−0.637	−1.015	0.909
Phosphate–SO_4^{2-}	10.99	0.039	−0.114	−0.499	−0.885	0.988
Phosphate–Ca(II)	14.57	0.055	−1.245	−1.794	−2.343	0.964
Phosphate–Mg(II)	13.54	0.049	−0.555	−1.045	−1.534	0.994

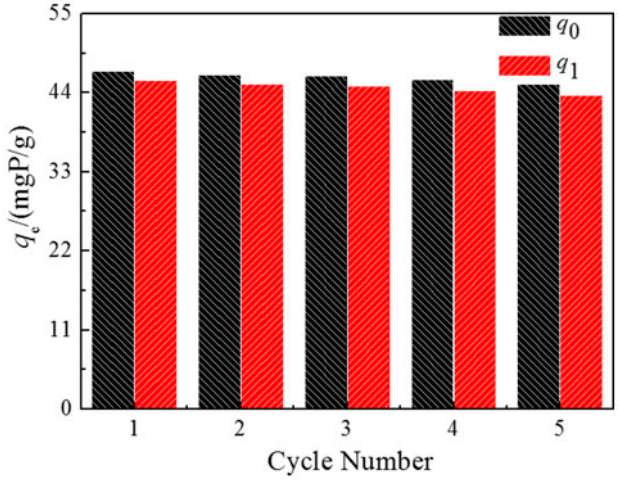

Fig. 10. Adsorption/desorption cycle of the DETA-PES membrane.

can provide three kinds of protonated sites, namely N_{34}, N_{37}, and N_{40} atoms (Fig. 2). Two kinds of condensed FF descriptors, namely, f_k^+ and f_k^- corresponding to an active site for nucleophile attack and electrophile attack, can be competent for revealing the protonated sites of the membrane. Herein, the value of f_k^+ is not shown, because DETA-PES chain of the membrane acts as a nucleophile in the protonation process. The values of f_k^- and the Mulliken atomic charges were assessed using the Mulliken population analysis and the technique of electrostatic potential derived charges, respectively. The protonation energy ($\Delta E(H^+)$) and the Gibbs free energies of protonation ($\Delta G(H^+)$) for the DETA-PES membrane were calculated via Eqs. (4)–(5) [32,34]:

$$\Delta E(H^+) = E((\text{DETA-PES-H})^+) + E(H_2O) - E(\text{DETA-PES}) - E(H_3O^+) \quad (4)$$

$$\Delta G(H^+) = \Delta E(H^+) + [G_{298}((\text{DETA-PES-H})^+) + G_{298}(H_2O) - G_{298}(\text{DETA-PES}) - G_{298}(H_3O^+)] \quad (5)$$

where $E(X)$ is the COSMO-corrected total energy of species (X), $G(X)$ is the computed temperature-corrected free energy of species (X) at 298 K. The calculated data are presented in Table 5.

The value of f_k^- (Table 5) is in the order of N_{34} < N_{37} < N_{40}, and the atomic charge of them also follows this order. Thus, N_{37} and N_{40} atoms are more easily protonated than N_{34}. Compared with that of N_{34} protonated membrane, the more negative values of ΔE (H^+) and ΔG (H^+) for N_{37} and N_{40} protonated forms also suggest that N_{37} and N_{40} atoms are easily protonated. Therefore, these two protonated geometries of the membrane, i.e. $(\text{DETA-PES-H}_{37})^+$ (protonation of N_{37}) and $(\text{DETA-PES-H}_{40})^+$ (protonation of N_{40}) are employed for the following calculations. The optimized conformations of them are shown in Fig. 11(a) and (b).

Unlike Cl^- and SO_4^{2-}, Ca(II) and Mg(II) can be coordinated by the nitrogen atoms of the DETA-PES affinity membrane to some extent [32]. The optimized structures of $[\text{M(II)(DETA-PES-H}_n)]^{3+}$ complexes are

Table 5
Calculated values of f_k^-, atomic charge, $\Delta E(H^+)$, and $\Delta G(H^+)$ for the protonation of nitrogen atoms

Atom	f_k^-	Atomic charge	ΔE (H^+)/(kJ/mol)	ΔG (H^+)/(kJ/mol)
N_{34}	0.012	–0.386	–0.543	0.623
N_{37}	0.138	–0.469	–28.66	–26.85
N_{40}	0.158	–0.488	–31.07	–28.57

presented in Fig. 11(c) and (d) (*n* denotes the protonated site of 37 or 40; M(II) represents Ca(II) or Mg (II)). When the N_{37} site of the DETA-PES membrane is protonated, both the bond lengths of N_{37}—Ca(II) and N_{37}—Mg(II) are more than 3.5 Å, indicating the nonexistence of bonding interactions between the N_{37} atom and these two cations. Hence, the [M(II)(DETA-PES-H_{37})]$^{3+}$ complexes will tend to exist in the form of 2-coordinated conformation. In addition, the [M(II)(DETA-PES-H_{40})]$^{3+}$ complexes also exhibit the 2-coordinated structures, because the bond lengths of N_{40}—Ca(II) and N_{40}—Mg(II) are higher than 4.0 Å.

3.6.2. Calculation of DFT reactivity descriptors

Calculated energies of highest occupied molecular orbital (E_{HOMO}), lowest unoccupied molecular orbital (E_{LUMO}), and the band gaps ($\Delta E_{LUMO\text{-}HOMO}$) of (DETA-PES-$H_n$)$^+$, [M(II)(DETA-PES-$H_n$)]$^{3+}$, $H_2PO_4^-$, HSO_4^-, and $[Cl(H_2O)_5]^-$ are shown in Table 6. Among them, (DETA-PES-H_n)$^+$ and [M(II)(DETA-PES-H_n)]$^{3+}$ have low LUMO energies and $H_2PO_4^-$ has a high HOMO energy, thus it can be confirmed that the affinities of (DETA-PES-H_n)$^+$ and [M(II)(DETA-PES-H_n)]$^{3+}$ to $H_2PO_4^-$ will be remarkable. The difference between E_{LUMO} of [Ca(II)(DETA-PES-H_{37})]$^{3+}$ and E_{HOMO} of $H_2PO_4^-$ is 0.077 Ha, which is smaller than that between other three [M(II)(DETA-PES-H_n)]$^{3+}$ complexes and phosphate. Also, this value is lower than the differences between E_{LUMO} of (DETA-PES-H_n)$^+$ and E_{HOMO} of $H_2PO_4^-$, HSO_4^-, and $Cl(H_2O)_5]^-$. Therefore, we believe that the electrostatic adsorption interaction between [Ca(II)(DETA-PES-H_{37}^+)]$^{3+}$ and $H_2PO_4^-$ is most notable.

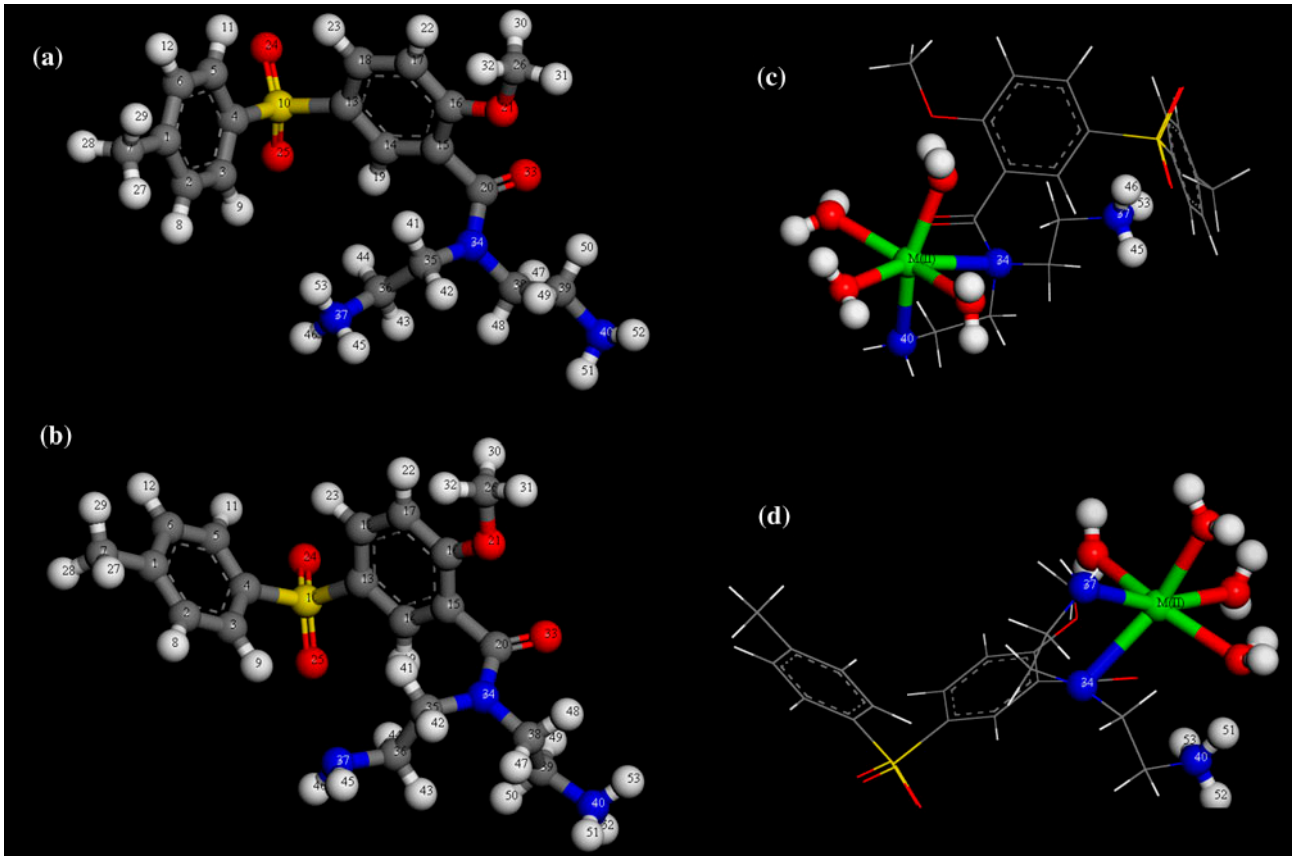

Fig. 11. Optimized structures of the protonated unit of DETA-PES membrane and its metal complex with the atoms numbering scheme adopted in this study: atom types are denoted by sequence number as follows: (a) (DETA-PES-H_{37})$^+$ (8, 9, 11, 12, 19, 22, 23, 27–32, 41–53—hydrogen; 1–7, 13–18, 20, 26, 35, 36, 38, 39—carbon; 21, 24, 25, 33—oxygen; 34, 37, 40—nitrogen; 10—sulfur), (b) (DETA-PES-H_{40})$^+$ (8, 9, 11, 12, 19, 22, 23, 27–32, 41–53—hydrogen; 1–7, 13–18, 20, 26, 35, 36, 38, 39—carbon; 21, 24, 25, 33—oxygen; 34, 37, 40—nitrogen; 10—sulfur), (c) [M(II)(DETA-PES-H_{37})]$^{3+}$ (M(II) represents Ca(II) or Mg(II); 45, 46, 53—hydrogen; 34, 37, 40—nitrogen), and (d) [M(II)(DETA-PES-H_{40})]$^{3+}$ (M(II) represents as Ca(II) or Mg(II); 51–53—hydrogen; 34, 37, 40—nitrogen).

Table 6
Calculated energies HOMO, LUMO, band gap ($\Delta E_{LUMO\text{-}HOMO}$), chemical potential ($\mu$), global hardness ($\eta$), and electrophilicity (ω) in Ha for the protonated DETA-PES, Ca(II)-, Mg(II)-loaded protonated DETA-PES, $H_2PO_4^-$, and the coexistent two anions

Reactant	E_{HOMO}	E_{LUMO}	$\Delta E_{LUMO\text{-}HOMO}$	μ	η	ω
$(DETA\text{-}PES\text{-}H_{37})^+$	−0.2043	−0.0808	0.1235	−0.1426	0.0618	0.1645
$(DETA\text{-}PES\text{-}H_{40})^+$	−0.2049	−0.0750	0.1299	−0.1400	0.0650	0.1508
$[Ca(II)(DETA\text{-}PES\text{-}H_{37})]^{3+}$	−0.2391	−0.1308	0.1083	−0.1850	0.0542	0.3157
$[Ca(II)(DETA\text{-}PES\text{-}H_{40})]^{3+}$	−0.2362	−0.1279	0.1083	−0.1821	0.0542	0.3059
$[Mg(II)(DETA\text{-}PES\text{-}H_{37})]^{3+}$	−0.2381	−0.1179	0.1202	−0.1780	0.0601	0.2636
$[Mg(II)(DETA\text{-}PES\text{-}H_{40})]^{3+}$	−0.2337	−0.1098	0.1239	−0.1718	0.0620	0.2380
$H_2PO_4^-$	−0.2078	0.0327	0.2405	−0.0876	0.1203	0.0319
HSO_4^-	−0.2140	0.0272	0.2412	−0.0934	0.1206	0.0362
$[Cl(H_2O)_5]^-$	−0.2278	0.0280	0.2558	−0.0999	0.1279	0.0390

The chemical activity descriptors involving chemical potential (μ), the global hardness (η), and the electrophilicity index (ω) of the above-reported nine species were defined by Eqs. (6)–(8) [32,58]:

$$\mu = \frac{(E_{HOMO} + E_{LUMO})}{2} \tag{6}$$

$$\eta = \frac{(E_{LUMO} - E_{HOMO})}{2} \tag{7}$$

$$\omega = \frac{\mu^2}{2\eta} \tag{8}$$

The calculated global reactivity descriptors for $(DETA\text{-}PES\text{-}H_n)^+$, $[M(II)(DETA\text{-}PES\text{-}H_n)]^{3+}$, $H_2PO_4^-$, HSO_4^-, and $[Cl(H_2O)_5]^-$ are also shown in Table 6. Values of chemical potential (μ) of $(DETA\text{-}PES\text{-}H_n)^+$ and $[M(II)(DETA\text{-}PES\text{-}H_n)]^{3+}$ are more negative than that of $H_2PO_4^-$, HSO_4^-, and $[Cl(H_2O)_5]^-$. In this sense, it can be inferred that both $(DETA\text{-}PES\text{-}H_n)^+$ and $[M(II)(DETA\text{-}PES\text{-}H_n)]^{3+}$ act as electrophiles (electron acceptors); while the three anions play the role of nucleophiles (electron donors). Among the electrophiles, the electronegativity (χ, $\chi = -\mu$) decreases in the order of $[Ca(II)(DETA\text{-}PES\text{-}H_{37})]^{3+}$ > $[Ca(II)(DETA\text{-}PES\text{-}H_{40})]^{3+}$ > $[Mg(II)(DETA\text{-}PES\text{-}H_{37})]^{3+}$ > $[Mg(II)(DETA\text{-}PES\text{-}H_{40})]^{3+}$ > $(DETA\text{-}PES\text{-}H_{37})^+$ > $(DETA\text{-}PES\text{-}H_{40})^+$. The $[Ca(II)(DETA\text{-}PES\text{-}H_{37})]^{3+}$ complex exhibits a stronger ability of obtaining electrons than other three $[M(II)(DETA\text{-}PES\text{-}H_n)]^{3+}$ complexes and the two $(DETA\text{-}PES\text{-}H_n)^+$ chains of the affinity membrane. In addition, values of μ and chemical hardness (η) for the N_{37} protonated membrane are more negative than those of the N_{40} protonated form, indicating that the N_{37} protonated membrane owns the high reactivity of accepting electrons. As to the aforementioned three nucleophiles, the values of χ and η follow the order of $H_2PO_4^-$ < HSO_4^- < $[Cl(H_2O)_5]^-$, suggesting that $H_2PO_4^-$ owns a stronger ability of donating electrons than HSO_4^- and $[Cl(H_2O)_5]^-$.

The calculated electrophilicity index (ω) of $(DETA\text{-}PES\text{-}H_n)^+$ and $[Ca(II)(DETA\text{-}PES\text{-}H_{37})]^{3+}$ is larger than that of $H_2PO_4^-$, HSO_4^- and $[Cl(H_2O)_5]^-$, coincident with the analysis of μ. For the six electrophiles, ω lines in the order trend: $[Ca(II)(DETA\text{-}PES\text{-}H_{37})]^{3+}$ > $[Ca(II)(DETA\text{-}PES\text{-}H_{40})]^{3+}$ > $[Mg(II)(DETA\text{-}PES\text{-}H_{37})]^{3+}$ > $[Mg(II)(DETA\text{-}PES\text{-}H_{40})]^{3+}$ > $(DETA\text{-}PES\text{-}H_{37})^+$ > $(DETA\text{-}PES\text{-}H_{40})^+$, indicating the enhancing effects of Ca(II) and Mg(II) on the phosphate uptake; the positive effect of Ca(II) is larger than that of Mg(II). ω of the nucleophiles follows the order of $H_2PO_4^-$ < HSO_4^- < $[Cl(H_2O)_5]^-$, and it suggests that the phosphate uptake of the membrane governs the adsorption process with the coexistence of Cl^- and SO_4^{2-}. Also, the interferential effect of SO_4^{2-} on phosphate adsorption higher than that of Cl^- can be deduced.

The intramolecular parameters of μ, η, and ω are only related to the properties of an isolated molecule. In comparison with them, the descriptor of charge transfer (ΔN) defined by Eq. (9) will be helpful in obtaining a complete picture of the adsorption process [24,58]:

$$\Delta N = \frac{(E^{B}_{HOMO} + E^{B}_{LOMO} - E^{A}_{HOMO} - E^{A}_{LUMO})}{2(E^{A}_{LUMO} + E^{B}_{LUMO} - E^{A}_{HOMO} - E^{B}_{HOMO})} \quad (9)$$

where superscripts of A and B are used to describe the reactants A and B, respectively. If $\Delta N < 0$, electrons will flow from A to B, i.e. A acts as the electron donor and B as electron acceptor. Furthermore, a high absolute value of ΔN between two molecules indicates the strong interaction of them [24,58]. ΔN values between $(DETA\text{-}PES\text{-}H_{37})^+$ and $H_2PO_4^-$, HSO_4^-, and $[Cl(H_2O)_5]^-$ are –0.1511, –0.1124, and –0.1348, respectively. And that between $(DETA\text{-}PES\text{-}H_{40})^+$ and the three anions mentioned above are –0.1415, –0.1055, and –0.1254. The negative value of ΔN indicates that $(DETA\text{-}PES\text{-}H_{37})^+$ and $(DETA\text{-}PES\text{-}H_{40})^+$ act as electrophiles, while $H_2PO_4^-$, HSO_4^-, and $[Cl(H_2O)_5]^-$ serve as nucleophiles. During the adsorption process, in contrast with Cl^- and SO_4^{2-}, phosphate shows a higher affinity with the DETA-PES affinity membrane. Compared with the amount of charge transfer between the membrane and Cl^- (ΔN ($[Cl(H_2O)_5]^- \rightarrow (DETA\text{-}PES\text{-}H_n)^+$)), the higher absolute value of ΔN ($HSO_4^- \rightarrow (DETA\text{-}PES\text{-}H_n)^+$) indicates that the interferential effect of SO_4^{2-} on phosphate adsorption is more remarkable than that of Cl^-. Values of ΔN between $H_2PO_4^-$ and $[Ca(II)(DETA\text{-}PES\text{-}H_{37})]^{3+}$, $[Ca(II)(DETA\text{-}PES\text{-}H_{40})]^{3+}$, $[Mg(II)(DETA\text{-}PES\text{-}H_{37})]^{3+}$, and $[Mg(II)(DETA\text{-}PES\text{-}H_{40})]^{3+}$ are –0.2792, –0.2709, –0.2508, and –0.2311, respectively. Based on this result, it can be believed that the coexistence of these two cations results in the enhancement in the phosphate uptake. Of course, in comparison with that of Mg(II), the more notably positive effect of Ca(II) on the phosphate adsorption can be validated.

3.6.3. The adsorption site of phosphate

As indicated by the optimized structure (Fig. 2(c)), the phosphate molecule can provide five adsorption sites, namely O_1, P_2, O_3, O_4, and O_5. In the adsorption process, phosphate acts as a nucleophile, so f_k^- will be suitable for revealing the reactive site of this species. The calculated f_k^- of these five sites are 0.324, 0.133, 0.321, –0.073, and 0.072. The atomic charges of them are –0.849, 1.464, –0.847, –0.662, and –0.662. Compared with those of other three sites, the more positive f_k^- and the more negative atomic charge of O_1 and O_3 sites suggest that these two sites are applicative for the interaction with the affinity membrane.

Considering the O_1 atom as the attacked site, the optimized geometries of $(DETA\text{-}PES\text{-}H_{37})^+$-$H_2PO_4^-$, $[M(II)(DETA\text{-}PES\text{-}H_{37})]^{3+}$-$H_2PO_4^-$, $(DETA\text{-}PES\text{-}H_{37})^+$-$HSO_4^-$, and $(DETA\text{-}PES\text{-}H_{37})^+$-$[Cl(H_2O)_5]^-$ are shown in Fig. 12. Herein, the optimized structures of the four N_{40}-based products were not shown, due to the similarities of them to the aforementioned four structures. Based on the same reason, the optimized geometry of phosphate adsorbed by the membrane via the O_3 site is omitted. As demonstrated by Fig. 12, the distances between O_1 ($H_2PO_4^-$), Cl ($[Cl(H_2O)_5]^-$), O_1 (HSO_4^-), and H_{53} ($(DETA\text{-}PES\text{-}H_{37})^+$) are 1.512, 2.194, and 1.499 Å, respectively. In this sense, the electrostatic attraction interactions between $(DETA\text{-}PES\text{-}H_{37})^+$ and the three anions are remarkable. Also, strong affinities of $[Ca(II)(DETA\text{-}PES\text{-}H_{37})]^{3+}$ and $[Mg(II)(DETA\text{-}PES\text{-}H_{37})]^{3+}$ to $H_2PO_4^-$ can be validated, because the bond lengths of O_1—Ca(II) and O_1—Mg(II) are 2.362 and 2.012 Å. In addition, the bonding interactions of $(DETA\text{-}PES\text{-}H_n)^+$ with $H_2PO_4^-$, $[Cl(H_2O)_5]^-$, HSO_4^-, and that of $[M(II)(DETA\text{-}PES\text{-}H_n)]^{3+}$ with $H_2PO_4^-$ are confirmed, because all distances between the protonated hydrogen ($(DETA\text{-}PES\text{-}H_n)^+$) and O_1 ($H_2PO_4^-$), O_3 ($H_2PO_4^-$), Cl ($[Cl(H_2O)_5]^-$), O_1 or O_4 (HSO_4^-), and that between M(II) ($(M(II)(DETA\text{-}PES\text{-}H_n)]^{3+}$) and O_3 or $O_1 + O_3$ ($H_2PO_4^-$) are smaller than 3.0 Å.

3.6.4. The adsorption energy and Gibbs free energy of adsorption

The adsorption energy (ΔE_{ads}) and Gibbs free energy of adsorption (ΔG_{ads}) at 298 K were calculated using Eqs. (10) and (11) [59]. ΔE_{ads} indicates the absorption capability of adsorbent toward adsorbate; the negative value of ΔG_{ads} will reflect the spontaneous characteristic of the adsorption process.

$$\Delta E_{ads} = \sum E(\text{product}) - \sum E(\text{reactant}) \quad (10)$$

$$\Delta G_{ads} = \Delta E_{ads} + (\sum G(\text{product}) - \sum G(\text{reactant})) \quad (11)$$

where $E(X)$ is the COSMO-corrected total energy of species (X). $G(X)$ is the computed temperature-corrected free energy of species (X) at 298 K.

The calculated ΔE_{ads} and ΔG_{ads} of $(DETA\text{-}PES\text{-}H_n)^+$-$H_2PO_4^-$, $[M(II)(DETA\text{-}PES\text{-}H_n)]^{3+}$-$H_2PO_4^-$, $(DETA\text{-}PES\text{-}H_n)^+$-$HSO_4^-$, and $(DETA\text{-}PES\text{-}H_n)^+$-$[Cl(H_2O)_5]^-$

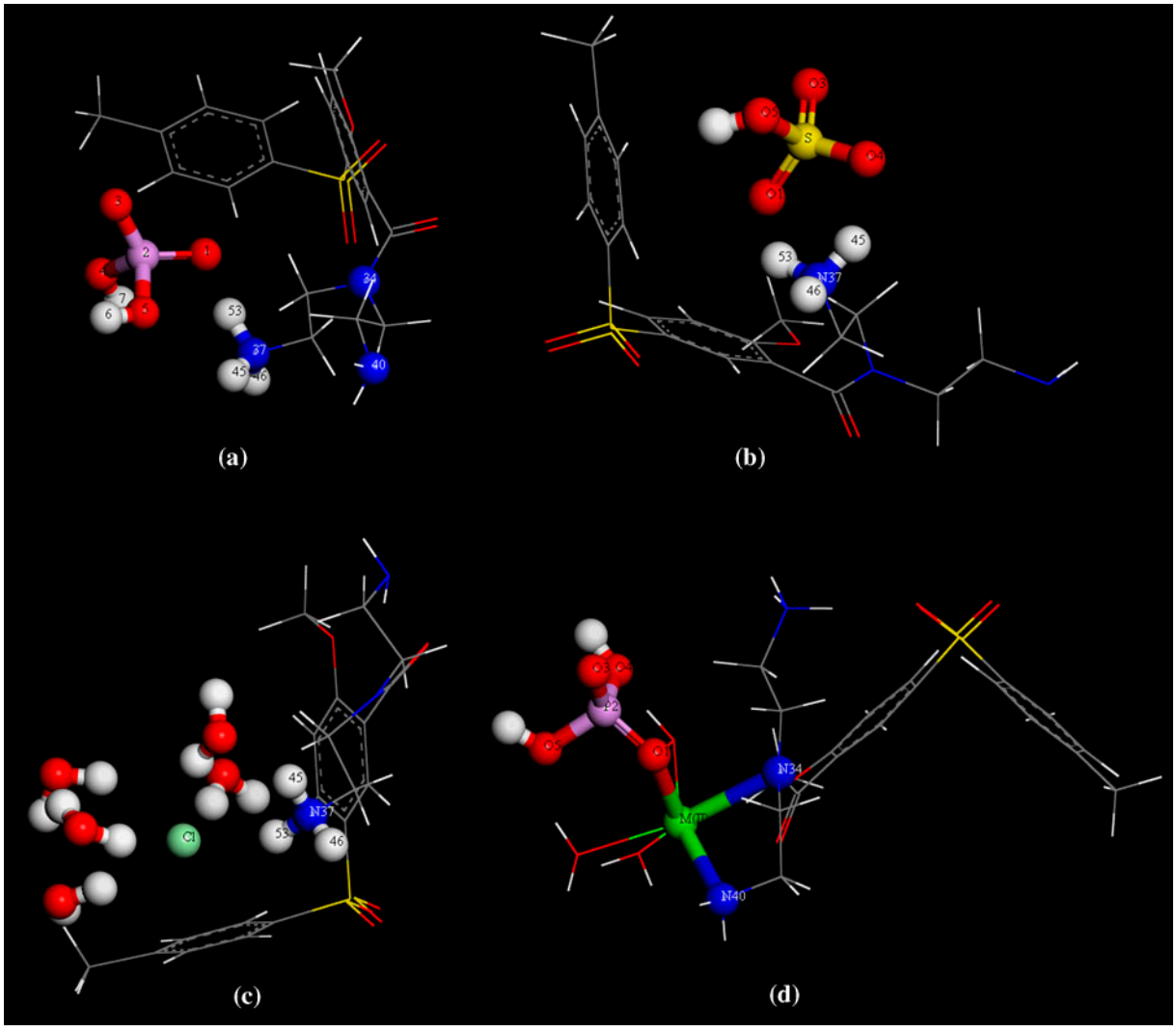

Fig. 12. Optimized structures of phosphate, SO_4^{2-}, and Cl^- adsorbed by DETA-PES-H_{37}^+, and that of phosphate adsorbed by M(II)(DETA-PES-H_{37}^+) with the atoms numbering scheme adopted in this study: atom types are denoted by sequence number as follows: (a) (DETA-PES-H_{37})$^+$-$H_2PO_4^-$ (6, 7, 45, 46, 53—hydrogen; 1, 3–5—oxygen; 34, 37, 40—nitrogen; 2–phosphorus), (b) (DETA-PES-H_{37})$^+$-HSO_4^- (45, 46, 53—hydrogen), (c) (DETA-PES-H_{37})$^+$-$[Cl(H_2O)_5]^-$ (45, 46, 53—hydrogen), and (d) [M(II)(DETA-PES-H_{37})]$^{3+}$-$H_2PO_4^-$ (M(II) represents as Ca(II) or Mg(II)).

complexes are shown in Table 7. ΔE_{ads} of (DETA-PES-H_n)$^+$-X (X represented as $H_2PO_4^-$, HSO_4^-, $[Cl(H_2O)_5]^-$) is in the order of $H_2PO_4^-$ > HSO_4^- > $[Cl(H_2O)_5]^-$, indicating that the DETA-PES membrane has a more notable affinity to phosphate than the coexistent Cl^- and SO_4^{2-}. Also, it can be concluded that SO_4^{2-} exerts a more negative effect on phosphate adsorption than Cl^-. ΔE_{ads} of the membrane toward these two coexistent anions cannot be comparable with that of phosphate.

In the presence of Ca(II) or Mg(II), three adsorption models involving M(II)-O_1, M(II)-O_3, and M(II)-O_1 + O_3 can be considered. ΔE_{ads} of [M(II)(DETA-PES-H_n)]$^{3+}$ toward phosphate via these three models lines in the order of M(II)-O_1 > M(II)-O_3 > M(II)-O_1 + O_3. Hence, the affinity of [M(II)(DETA-PES-H_n)]$^{3+}$ toward phosphate via the model of M(II)-O_1 is the most remarkable. When the O_1 atom of phosphate is applied as the adsorption site, ΔE_{ads} of (DETA-PES-H_n)$^+$ and [M(II)(DETA-PES-H_n)]$^{3+}$ toward phosphate follows the order: [Ca(II)(DETA-PES-H_{37})]$^{3+}$ > [Ca(II)(DETA-PES-H_{40})]$^{3+}$ > [Mg(II)(DETA-PES-H_{37})]$^{3+}$ > [Mg(II)(DETA-PES-H_{40})]$^{3+}$ > (DETA-PES-H_{37})$^+$ > (DETA-PES-H_{40})$^+$, which is in accordance with experimental analyses. The enhancing effect of Ca(II) on the phosphate uptake is larger than that of Mg(II). Thus, based

Table 7
Calculated adsorption energies and adsorbing Gibbs free energies of $(DETA\text{-}PES\text{-}H_n)^+$ interacting with $H_2PO_4^-$, Cl^-, SO_4^{2-}, and that of $[M(II)(DETA\text{-}PES\text{-}H_n)]^{3+}$ interacting with $H_2PO_4^-$

	$H_2PO_4^-$			Cl^-		SO_4^{2-}	
Species	Site	ΔE_{ads} (kJ/mol)	ΔG_{ads} (kJ/mol)	ΔE_{ads} (kJ/mol)	ΔG_{ads} (kJ/mol)	ΔE_{ads} (kJ/mol)	ΔG_{ads} (kJ/mol)
$(DETA\text{-}PES\text{-}H_{37})^+$	O_1	–20.78	–5.92	–6.05	–12.72	–16.24	–2.93
	O_3	–20.85	–7.47				
$(DETA\text{-}PES\text{-}H_{40})^+$	O_1	–15.29	–3.10	–0.23	–5.88	–11.10	–4.77
	O_3	–15.79	–4.26				
$[Ca(II)(DETA\text{-}PES\text{-}H_{37})]^{3+}$	O_1	–22.05	–18.86	–	–	–	–
	O_3	–20.03	–13.42				
	$O_1 + O_3$	–13.84	–22.37				
$[Ca(II)(DETA\text{-}PES\text{-}H_{40})]^{3+}$	O_1	–22.58	–16.20	–	–	–	–
	O_3	–18.98	–14.99				
	$O_1 + O_3$	–13.80	–21.52				
$[Mg(II)(DETA\text{-}PES\text{-}H_{37})]^{3+}$	O_1	–21.17	–18.79	–	–	–	–
	O_3	–19.71	–19.04				
	$O_1 + O_3$	–7.8	–20.04				
$[Mg(II)(DETA\text{-}PES\text{-}H_{40})]^{3+}$	O_1	–20.84	–16.72	–	–	–	–
	O_3	–17.24	–15.45				
	$O_1 + O_3$	–6.63	–11.21				

on this fact, after loading metal ions, the performance in phosphate uptake of the DETA-PES affinity membrane will be enhanced.

4. Conclusions

The fabricated DETA-PES membrane was employed to remove phosphate from the solutions. Batch adsorption experiments and DFT calculations were applied to evaluate the characteristics of phosphate adsorption by the membrane. In addition, influences of the coexistent Cl^-, SO_4^{2-}, Ca(II), and Mg(II) on phosphate uptake of the membrane were revealed. The conclusions are shown as follows:

(1) Results of DFT simulation are in accordance with the experiment data, indicating that DFT molecular simulation is competent for evaluating the adsorption process between DETA-PES affinity membrane and phosphate.
(2) The coexistent SO_4^{2-} exhibits a much more negative influence on phosphate uptake than Cl^-. Also, the positive influence of Ca(II) on phosphate adsorption is more remarkable than that of Mg(II).
(3) The coexistence of the four ions does not alter the nature of the membrane toward phosphate. Lagergren second-order model is competent for describing the adsorption kinetic of the membrane, and the adsorption isotherms can be well described by Langmuir model. The adsorption of phosphate onto the membrane is a spontaneous, endothermic process. The chemisorption interaction between the membrane and phosphate plays an important role in the uptake of this pollutant.
(4) The affinity of the protonated DETA-PES membrane to phosphate is stronger than that to Cl^- and SO_4^{2-}, due to the maximum charge transfer between phosphate and the $(DETA\text{-}PES\text{-}H_n)^+$ chain, and the more negative adsorption energy and Gibbs free energy of adsorption for the formed $(DETA\text{-}PES\text{-}H_n)^+\text{-}H_2PO_4^-$ complex.
(5) The coexistent Ca(II) and Mg(II) can be coordinated by the affinity membrane. The large amount of charge transfer, the noticeably negative adsorption energy and Gibbs free energy of adsorption for the $[M(II)(DETA\text{-}PES\text{-}H_n)]^{3+}\text{-}H_2PO_4^-$ complexes, suggests that the Ca(II)-, and Mg(II)-loaded affinity membrane is more suitable for the removal of phosphate than that without loading these two metals.

Acknowledgment

This work was supported by the Scientific Research Foundation of the Hebei Higher Education Institutions of China (Grant No. ZD2015120).

References

[1] D.Y. Zhao, A.K. Sengupta, Ultimate removal of phosphate from wastewater using a new class of polymeric ion exchangers, Water Res. 32 (1998) 1613–1625.

[2] A. Mullan, J.W. McGrath, T. Adamson, S. Irwin, J.P. Quinn, Pilot-scale evaluation of the application of low pH-inducible polyphosphate accumulation to the biological removal of phosphate from wastewaters, Environ. Sci. Technol. 40 (2006) 296–301.

[3] S. Pitois, M.H. Jackson, B.J.B. Wood, Problems associated with the presence of cyanobacteria in recreational and drinking waters, Int. J. Environ. Health Res. 10 (2000) 203–218.

[4] P.P. Shen, Q. Shi, Z.C. Hua, F.X. Kong, Z.G. Wang, S.X. Zhuang, D.C. Chen, Analysis of microcystins in cyanobacteria blooms and surface water samples from Meiliang Bay, Taihu Lake, China, Environ. Int. 29 (2003) 641–647.

[5] H. Deng, X.L. Yu, Adsorption of fluoride, arsenate and phosphate in aqueous solution by cerium impregnated fibrous protein, Chem. Eng. J. 184 (2012) 205–212.

[6] D. Mulkerrins, A.D.W. Dobson, E. Colleran, Parameters affecting biological phosphate removal from wastewaters, Environ. Int. 30 (2004) 249–259.

[7] N.O. Yigit, S. Mazlum, Phosphate recovery potential from wastewater by chemical precipitation at batch conditions, Environ. Technol. 28 (2007) 83–93.

[8] J.P. Chen, M.L. Chua, B.P. Zhang, Effects of competitive ions, humic acid, and pH on removal of ammonium and phosphorous from the synthetic industrial effluent by ion exchange resins, Waste Manage. 22 (2002) 711–719.

[9] T. Nur, M.A.H. Johir, P. Loganathan, S. Vigneswaran, J. Kandasamy, Effectiveness of purolite A500PS and A520E ion exchange resins on the removal of nitrate and phosphate from synthetic water, Desalin. Water Treat. 47 (2012) 50–58.

[10] W.-Y. Huang, D. Li, J. Yang, Z.-Q. Liu, Y. Zhu, Q. Tao, K. Xu, J.-Q. Li, Y.-M. Zhang, One-pot synthesis of Fe(III)-coordinated diamino-functionalized mesoporous silica: Effect of functionalization degrees on structures and phosphate adsorption, Microporous Mesoporous Mater. 170 (2013) 200–210.

[11] L.-G. Yan, Y.-Y. Xu, H.-Q. Yu, X.-D. Xin, Q. Wei, B. Du, Adsorption of phosphate from aqueous solution by hydroxy-aluminum, hydroxy-iron and hydroxy-iron-aluminum pillared bentonites, J. Hazard. Mater. 179 (2010) 244–250.

[12] A. Ugurlu, B. Salman, Phosphorus removal by fly ash, Environ. Int. 24 (1998) 911–918.

[13] M.S. Onyango, D. Kuchar, M. Kubota, H. Matsuda, Adsorptive removal of phosphate ions from aqueous solution using synthetic zeolite, Ind. Eng. Chem. Res. 46 (2007) 894–900.

[14] K. Karageorgiou, M. Paschalis, G.N. Anastassakis, Removal of phosphate species from solution by adsorption onto calcite used as natural adsorbent, J. Hazard. Mater. 139 (2007) 447–452.

[15] X.M. Wang, W. Li, R. Harrington, F. Liu, J.B. Parise, X.H. Feng, D.L. Sparks, Effect of ferrihydrite crystallite size on phosphate adsorption reactivity, Environ. Sci. Technol. 47 (2013) 10322–10331.

[16] J.-H. Yuan, M.-H. Hu, Z.-H. Zhou, L. Wang, Kinetic and thermodynamic behavior of the batch adsorption of phosphate from aqueous solutions onto environmentally friendly barbecue bamboo charcoal, Desalin. Water Treat. 52 (2014) 7248–7257.

[17] P.R. Rout, P. Bhunia, R.R. Dash, A mechanistic approach to evaluate the effectiveness of red soil as a natural adsorbent for phosphate removal from wastewater, Desalin. Water Treat. 54 (2015) 358–373.

[18] T.S. Anirudhan, T.A. Rauf, S.R. Rejeena, Removal and recovery of phosphate ions from aqueous solutions by amine functionalized epichlorohydrin-grafted cellulose, Desalination 285 (2012) 277–284.

[19] Md.R. Awual, A. Jyo, T. Ihara, N. Seko, M. Tamada, K.T. Lim, Enhanced trace phosphate removal from water by zirconium(IV) loaded fibrous adsorbent, Water Res. 45 (2011) 4592–4600.

[20] A. Sowmya, S. Meenakshi, Effective utilization of the functional groups in chitosan by loading Zn(II) for the removal of nitrate and phosphate, Desalin. Water Treat. 54 (2015) 1674–1683.

[21] G. Arthanareeswaran, P. Thanikaivelan, J.A. Raguime, M. Raajenthiren, D. Mohan, Metal ion separation and protein removal from aqueous solutions using modified cellulose acetate membranes: Role of polymeric additives, Sep. Purif. Technol. 55 (2007) 8–15.

[22] B. Kalbfuss, M. Wolff, L. Geisler, A. Tappe, R. Wickramasinghe, V. Thom, U. Reichl, Direct capture of influenza A virus from cell culture supernatant with Sartobind anion-exchange membrane adsorbers, J. Membr. Sci. 299 (2007) 251–260.

[23] N. Flores-Holguín, A. Aguilar-Elguézabal, L.M. Rodríguez-Valdez, D. Glossman-Mitnik, Theoretical study of chemical reactivity of the main species in the α-pinene isomerization reaction, J. Mol. Struct. THEOCHEM 854 (2008) 81–88.

[24] A. Srivastava, P. Rawat, P. Tandon, R.N. Singh, A computational study on conformational geometries, chemical reactivity and inhibitor property of an alkaloid bicuculline with γ-aminobutyric acid (GABA) by DFT, Comput. Theor. Chem. 993 (2012) 80–89.

[25] I.S.P. Savizi, M.J. Janik, Acetate and phosphate anion adsorption linear sweep voltammograms simulated using density functional theory, Electrochim. Acta 56 (2011) 3996–4006.

[26] R. Rahnemaie, T. Hiemstra, W.H. van Riemsdijk, Carbonate adsorption on goethite in competition with phosphate, J. Colloid Interface Sci. 315 (2007) 415–425.

[27] N.Y. Acelas, S.M. Mejia, F. Mondragón, E. Flórez, Density functional theory characterization of phosphate and sulfate adsorption on Fe-(hydr)oxide: Reactivity, pH effect, estimation of Gibbs free energies, and topological analysis of hydrogen bonds, Comput. Theor. Chem. 2013 (1005) 16–24.

[28] X.M. Ren, S.T. Yang, X.L. Tan, C.L. Chen, G.D. Sheng, X.K. Wang, Mutual effects of copper and phosphate

on their interaction with γ-Al_2O_3: Combined batch macroscopic experiments with DFT calculations, J. Hazard. Mater. 237–238 (2012) 199–208.
[29] C.S. Zhao, X.S. Zhou, Y.L. Yue, Determination of pore size and pore size distribution on the surface of hollow-fiber filtration membranes: A review of methods, Desalination 129 (2000) 107–123.
[30] L.S. Čerović, S.K. Milonjić, M.B. Todorović, M.I. Trtanj, Y.S. Pogozhev, Y. Blagoveschenskii, E.A. Levashov, Point of zero charge of different carbides, Colloids Surf. A: Physicochem. Eng. Aspects 297 (2007) 1–6.
[31] K. Rezaei, H. Nedjate, Diluent effect on the distribution ratio and separation factor of Ni(II) in the liquid-liquid extraction from aqueous acidic solutions using dibutyldithiophosphoric acid, Hydrometallurgy 68 (2003) 11–21.
[32] L.Z. Song, M. Yang, J. Fu, P.P. Lu, X.L. Wang, J. He, Adsorption performance of APTMS-DTPA/PVDF chelating membrane toward Ni(II) with the presence of Ca(II), NH_4^+, lactic acid, and citric acid, Desalin. Water Treat. 53 (2015) 158–170.
[33] X.D. Zhao, L.Z. Song, J. Fu, P. Tang, F. Liu, Adsorption characteristics of Ni(II) onto MA–DTPA/PVDF chelating membrane, J. Hazard. Mater. 189 (2011) 732–740.
[34] X.D. Zhao, L.Z. Song, Z.H. Zhang, R. Wang, J. Fu, Adsorption investigation of MA-DTPA chelating resin for Ni(II) and Cu(II) using experimental and DFT methods, J. Mol. Struct. 986 (2011) 68–74.
[35] C. Magnenet, F.E. Jurin, S. Lakard, C.C. Buron, B. Lakard, Polyelectrolyte modification of ultrafiltration membrane for removal of copper ions, Colloids Surf. A: Physicochem. Eng. Aspects 435 (2013) 170–177.
[36] A. Rezvani-Boroujeni, M. Javanbakht, M. Karimi, C. Shahrjerdi, B. Akbari-adergani, Immoblization of thiol-functionalized nanosilica on the surface of poly(ether sulfone) membranes for the removal of heavy-metal ions from industrial wastewater samples, Ind. Eng. Chem. Res. 54 (2015) 502–513.
[37] J. Dai, H. Yang, H. Yan, Y.G. Shangguan, Q. Zheng, R.S. Cheng, Phosphate adsorption from aqueous solutions by disused adsorbents: Chitosan hydrogel beads after the removal of copper(II), Chem. Eng. J. 166 (2011) 970–977.
[38] J.D. Zhang, Z.M. Shen, W.P. Shan, Z.J. Mei, W.H. Wang, Adsorption behavior of phosphate on lanthanum(III)-coordinated diamino-functionalized 3D hybrid mesoporous silicates material, J. Hazard. Mater. 186 (2011) 76–83.
[39] K.M. Knauer, B.M. Greenhoe, J.S. Wiggins, S.E. Morgan, Surface composition control via chain end segregation in polyethersulfone solution cast films, Polymer 57 (2015) 88–98.
[40] B.H. Fang, Q.Y. Ling, W.F. Zhao, Y.L. Ma, P.L. Bai, Q. Wei, H.F. Li, C.S. Zhao, Modification of polyethersulfone membrane by grafting bovine serum albumin on the surface of polyethersulfone/poly(acrylonitrile-co-acrylic acid) blended membrane, J. Membr. Sci. 329 (2009) 46–55.
[41] A. Ananth, G. Arthanareeswaran, A.F. Ismail, Y.S. Mok, T. Matsuura, Effect of bio-mediated route synthesized silver nanoparticles for modification of polyethersulfone membranes, Colloids Surf. A: Physicochem. Eng. Aspects 451 (2014) 151–160.
[42] E. Kobayashi, M. Ando, Y. Tsutsumi, H. Doi, T. Yoneyama, M. Kobayashi, T. Hanawa, Inhibition effect of zirconium coating on calcium phosphate precipitation of titanium to avoid assimilation with bone, Mater. Trans. 48 (2007) 301–306.
[43] Y. Zhang, X.Q. Xi, S.N. Xu, J.C. Zhou, J.J. Zhou, Q.H. Xu, H.Y. Shen, Adsorption studies on phosphate by amino-functionalized nano-size composite materials, Acta Chim. Sinica 70 (2012) 1839–1846.
[44] G.M. Xu, Z. Shi, J. Deng, Characterization of adsorption of antimony and phosphate by using IOCS with XRD, FTIR and XPS, Acta Sci. Circumst. 27 (2007) 402–407.
[45] W. Mabrouk, L. Ogier, S. Vidal, C. Sollogoub, F. Matoussi, M. Dachraoui, J.F. Fauvarque, Synthesis and characterization of polymer blends of sulfonated polyethersulfone and sulfonated polyethersulfone octylsulfonamide for PEMFC applications, Fuel Cells 12 (2012) 179–187.
[46] D.P. Lu, H. Zou, R. Guan, H. Dai, L. Lu, Sulfonation of polyethersulfone by chlorosulfonic acid, Polym. Bull. 54 (2005) 21–28.
[47] W. Li, A.-M. Pierre-Louis, K.D. Kwon, J.D. Kubicki, D.R. Strongin, B.L. Phillips, Molecular level investigations of phosphate sorption on corundum (α-Al_2O_3) by 31P solid state NMR, ATR-FTIR and quantum chemical calculation, Geochim. et Cosmochim. Acta 107 (2013) 252–266.
[48] S.A. Kang, W. Li, H.E. Lee, B.L. Phillips, Y.J. Lee, Phosphate uptake by TiO_2: Batch studies and NMR spectroscopic evidence for multisite adsorption, J. Colloid Interface Sci. 364 (2011) 455–461.
[49] B. Saha, S. Chakraborty, G. Das, A mechanistic insight into enhanced and selective phosphate adsorption on a coated carboxylated surface, J. Colloid Interface Sci. 331 (2009) 21–26.
[50] J.Y. Liu, L.H. Wan, L. Zhang, Q. Zhou, Effect of pH, ionic strength, and temperature on the phosphate adsorption onto lanthanum-doped activated carbon fiber, J. Colloid Interface Sci. 364 (2011) 490–496.
[51] L.A. Rodrigues, M.L.C.P.D. Silva, Thermodynamic and kinetic investigations of phosphate adsorption onto hydrous niobium oxide prepared by homogeneous solution method, Desalination 263 (2010) 29–35.
[52] Y.S. Ho, G. McKay, A comparison of chemisorption kinetic models applied to pollutant removal on various sorbents, Process Saf. Environ. Prot. 76 (1998) 332–340.
[53] L.J. Li, F.Q. Liu, X.S. Jing, P.P. Ling, A.M. Li, Displacement mechanism of binary competitive adsorption for aqueous divalent metal ions onto a novel IDA-chelating resin: Isotherm and kinetic modeling, Water Res. 45 (2011) 1177–1188.
[54] B.P. Bering, M.M. Dubinin, V.V. Serpinsky, On thermodynamics of adsorption in micropores, J. Colloid Interface Sci. 38 (1972) 185–194.
[55] X. Huang, X.P. Liao, B. Shi, Adsorption removal of phosphate in industrial wastewater by using metal-loaded skin split waste, J. Hazard. Mater. 166 (2009) 1261–1265.

[56] Y. Yao, B. Gao, M.D. Inyang, A.R. Zimmerman, X.D. Cao, P. Pullammanappallil, L.Y. Yang, Removal of phosphate from aqueous solution by biochar derived from anaerobically digested sugar beet tailings, J. Hazard. Mater. 190 (2011) 501–507.
[57] G.S. Zhang, H.J. Liu, R.P. Liu, J.H. Qu, Removal of phosphate from water by a Fe–Mn binary oxide adsorbent, J. Colloid Interface Sci. 335 (2009) 168–174.
[58] V. Kumar, G. Jain, S. Kishor, L.M. Ramaniah, Chemical reactivity analysis of some alkylating drug molecules—A density functional theory approach, Comput. Theor. Chem. 968 (2011) 18–25.
[59] X.D. Zhao, L.Z. Song, J. Fu, P. Tang, F. Liu, Experimental and DFT investigation of surface degradation of polyvinylidene fluoride membrane in alkaline solution, Surf. Sci. 605 (2011) 1005–1015.